AD-A136 390   COMBUSTION OF AGGLOMERATES FORMED BY CARBON SLURRY   1/2
FUELS(U) PENNSYLVANIA STATE UNIV UNIVERSITY PARK DEPT
OF MECHANICAL ENGINEERING S R TURNS ET AL. NOV 83
UNCLASSIFIED   AFWAL-TR-83-2076 F33615-82-K-2256   F/G 21/2   NL

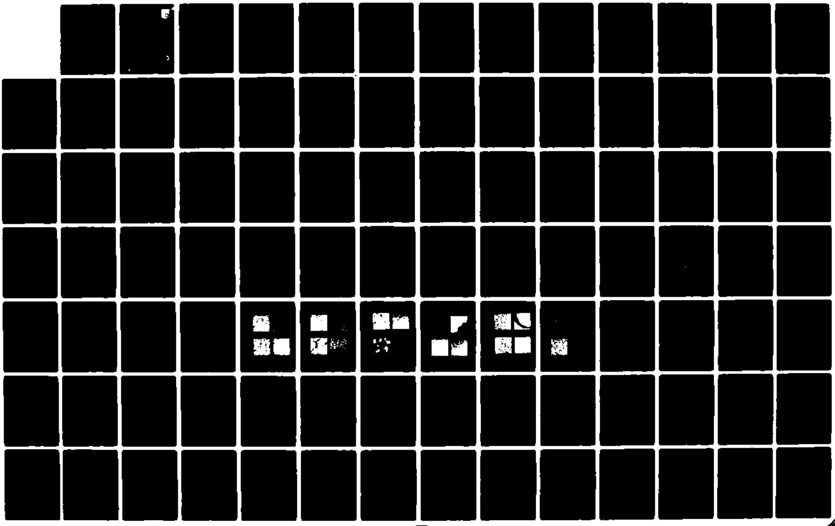

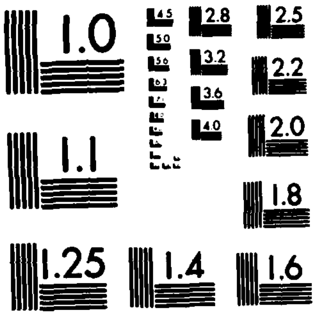

MICROCOPY RESOLUTION TEST CHART
NATIONAL BUREAU OF STANDARDS-1963-A

12

AFWAL-TR-83-2076

COMBUSTION OF AGGLOMERATES FORMED BY CARBON SLURRY FUELS

S. R. Turns, S. P. Riddle and G. M. Faeth

The Pennsylvania State University
Department of Mechanical Engineering
University Park, PA 16802

November 1983

Final Report for Period July 1982 - September 1983

Approved for public release; distribution unlimited

AERO PROPULSION LABORATORY
AIR FORCE WRIGHT AERONAUTICAL LABORATORIES
AIR FORCE SYSTEMS COMMAND
WRIGHT-PATTERSON AIR FORCE BASE, OHIO 45433

A136390

DTIC FILE COPY

DTIC
SELECTE
DEC 29 1983
D
E

83 12 29 030

NOTICE

When Government drawings, specifications, or other data are used for any purpose other than in connection with a definitely related Government procurement operation, the United States Government thereby incurs no responsibility nor any obligation whatsoever; and the fact that the government may have formulated, furnished, or in any way supplied the said drawings, specifications, or other data, is not to be regarded by implication or otherwise as in any manner licensing the holder or any other person or corporation, or conveying any rights or permission to manufacture use, or sell any patented invention that may in any way be related thereto.

This report has been reviewed by the Office of Public Affairs (ASD/PA) and is releasable to the National Technical Information Service (NTIS). At NTIS, it will be available to the general public, including foreign nations.

This technical report has been reviewed and is approved for publication.

Charles R. Martel
CHARLES R. MARTEL
Technical Area Manager
Fuels Branch
Fuels and Lubrication Division
Aero Propulsion Laboratory

Arthur V. Churchill
ARTHUR V. CHURCHILL
Chief, Fuels Branch
Fuels and Lubrication Division
Aero Propulsion Laboratory

FOR THE COMMANDER

Benito P. Botteri
BENITO P. BOTTERI
Asst Chief, Fuels and Lubrication Division
Aero Propulsion Laboratory

"If your address has changed, if you wish to be removed from our mailing list, or if the addressee is no longer employed by your organization please notify C. Martel *,* AFWAL/POSF *W-PAFB, OH 45433 to help us maintain a current mailing list".*

Copies of this report should not be returned unless return is required by security considerations, contractual obligations, or notice on a specific document.

REPORT DOCUMENTATION PAGE

READ INSTRUCTIONS BEFORE COMPLETING FORM

1. REPORT NUMBER
AFWAL-TR-83-2076

2. GOVT ACCESSION NO.
AD-A136390

3. RECIPIENT'S CATALOG NUMBER

4. TITLE (*and Subtitle*)
Combustion of Agglomerates Formed by Carbon Slurry Fuels

5. TYPE OF REPORT & PERIOD COVERED
Final Report for Period
July 1982-September 1983

6. PERFORMING ORG. REPORT NUMBER

7. AUTHOR(s)
S. R. Turns, S. P. Riddle and G. M. Faeth

8. CONTRACT OR GRANT NUMBER(s)
F33615-82-K-2256

9. PERFORMING ORGANIZATION NAME AND ADDRESS
The Pennsylvania State University
Department of Mechanical Engineering
University Park, PA 16802

10. PROGRAM ELEMENT, PROJECT, TASK AREA & WORK UNIT NUMBERS
PE-62203F
3048 05 19

11. CONTROLLING OFFICE NAME AND ADDRESS
Aero Propulsion Laboratory (AFWAL/POSF)
AF Wright Aeronautical Laboratories, AFSC
Wright-Patterson Air Force Base, OH 45433

12. REPORT DATE
November 1983

13. NUMBER OF PAGES
88

14. MONITORING AGENCY NAME & ADDRESS (*if different from Controlling Office*)

15. SECURITY CLASS. (*of this report*)
Unclassified

15a. DECLASSIFICATION/DOWNGRADING SCHEDULE

16. DISTRIBUTION STATEMENT (*of this Report*)
Approved for public release; distribution unlimited.

17. DISTRIBUTION STATEMENT (*of the abstract entered in Block 20, if different from Report*)

18. SUPPLEMENTARY NOTES

19. KEY WORDS (*Continue on reverse side if necessary and identify by block number*)
Carbon Slurry
High Density Fuels
Slurry Fuels
Slurry Combustion
Carbon Combustion

20. ABSTRACT (*Continue on reverse side if necessary and identify by block number*)

A theoretical and experimental study of the reaction of carbon-black agglomerates, which are formed during the combustion of carbon-black slurry fuels, is reported. Theoretical work includes development of a one-dimensional model of a carbon slurry-fueled combustor in order to gain insight concerning effects of slurry properties and combustor operating conditions on combustor performance. New experiments were also undertaken in order to study

Block 20 - ABSTRACT (Continued)

effects of carbon-black composition and catalyst loading on agglomerate burning rates.

The one-dimensional combustor model incorporates a shrinking-sphere analysis of agglomerate combustion developed earlier in this laboratory. The agglomerate combustion model uses a $C-O_2-CO_2-H_2O$ reaction mechanism combined with empirical area-reactivity and transport-enhancement factors which treat effects of pores in the agglomerate. To provide guidelines for combustor design, calculations were performed to find the effects of initial agglomerate diameter, combustor pressure, secondary air scheduling, reference velocity (or mass loading), the presence of catalyst and carbon-black blend on combustor performance. Major findings are: (1) reducing initial agglomerate size significantly improves combustor performance while effects of carbon-black blend and catalyst are small, suggesting that fuel development efforts should concentrate on properties which improve atomization; (2) combustor performance improves with increasing pressure, particularly in the range 1-10 atm.; (3) rapid introduction of secondary air does not quench agglomerate combustion but increases performance for typical operating conditions; and (4) increased reference velocities reduce performance in a manner consistent with reduced agglomerate residence times. Effects of agglomerate slip velocity and preheat upon emerging from the primary zone were also studied, since these quantities appear in the analysis as unknown initial conditions. It was found that the computations are relatively insensitive to levels of preheat, but that agglomerate slip velocity has a substantial effect on combustor performance and should be studied further. Simplified scaling laws for percent carbon burnout are also developed to assist interpretation of combustor performance measurements.

The new experiments considered agglomerates having initial diameters of roughly 750 μm supported in the post-flame region of a flat-flame burner in order to simulate combustor conditions. The test range included various levels of diffusion- and kinetic-control of the reaction mechanism. Both neat samples and blends of carbon blacks having ultimate carbon particle sizes (d_u) of 70, 180 and 350 nm were studied. The effect of lead catalyst was also considered. At all conditions, burning rates were fastest for $d_u = 70$ nm and progressively decreased (generally in the range 10-40%) as material with larger d_u was added to the blend. Addition of lead catalyst increased burning rates by as much as a factor of two, particularly in the range 0-0.25 g Pb/kg C. However, all these effects were greatest at kinetic-controlled conditions, which the one-dimensional analysis indicates is not of major importance for combustor operating conditions. It is concluded that major fuel formulation efforts should concentrate on improving the atomization quality of carbon-black slurries--as opposed to efforts to increase fundamental agglomerate reactivity.

SUMMARY

A theoretical and experimental study of the reaction of carbon-black agglomerates, which are formed during the combustion of carbon-black slurry fuels, is described. The theoretical work includes development of a one-dimensional model of a carbon slurry-fueled combustor in order to gain insight concerning effects of slurry properties and combustor operating conditions on combustor performance. The experiments examine effects of carbon-black composition and catalyst on agglomerate burning rates for environments representative of practical combustion chamber conditions. The main features of each portion of the study are described in the following.

Theory. A one-dimensional model of a carbon slurry-fueled combustor was developed. This model assumed that the relatively slow burning carbon agglomerates, formed by the evaporation of the liquid fuel component from the slurry fuel droplets, survive the primary combustion zone and burn out in a secondary zone consisting of agglomerate particles and products of combustion. The model allows specification of any arbitrary secondary air schedule. Mixing rates among the secondary air, particle products of combustion and bulk gas were assumed to be infinitely fast. The model incorporated a previously developed shrinking-sphere agglomerate combustion analysis which utilizes a C-O_2-CO_2-H_2O reaction mechanism combined with empirical area-reactivity and transport enhancement factors.

This one-dimensional model was used in a parametric study to provide guidelines for practical combustor design. The effects of initial carbon agglomerate size, chamber pressure, secondary air schedule, reference velocity, initial agglomerate temperature, initial slip velocity, and slurry variables on combustor performance were evaluated. Results showed that initial agglomerate diameter, chamber pressure, and secondary air scheduling all had a significant effect on carbon burnout. The effects of diameter and pressure were essentially independent of the extent of reaction or combustion efficiency, while the effect of early air introduction diminished to near zero as combustion efficiencies approached 100%. Increasing combustor reference velocity strongly affected carbon burnout lengths through the combined effects of decreased residence time--causing increased burnout length--and a more oxygen-rich environment for a fixed air injection length--which counteracted the residence time effect to some degree. Burnout times were significantly decreased by the oxygen enrichment effect. The effect of particle preheat was relatively insignificant for combustion efficiencies of practical importance; however, variations in initial particle slip velocity produced a substantial effect on predicted combustor performance and should be investigated further. The predicted effects of changing ultimate carbon particle size and addition of catalyst on combustor performance were insignificant, indicating the unimportance of agglomerate microstructure details and reactivity in

diffusion-controlled combustion environments which are normally encountered in practice.

Experiment. The experiments considered pre-dried agglomerates, having initial diameters of roughly 750 μm, supported in the post-flame region of a flat-flame burner. The burner was operated at atmospheric pressure with fuel equivalence ratios of 0.6 and 1.0 and temperatures of 1690 and 1940K. Gas compositions were measured with a gas chromatograph, gas temperatures were measured with a fine-wire thermocouple corrected for radiation errors, and gas velocities were computed from these properties assuming one-dimensional flow. Particle diameters were measured as a function of residence time in the burner gas. These data were processed to yield burning rates. Particle densities were also measured. Neat samples and blends of carbon blacks having ultimate carbon particle sizes of 70, 180 and 350 nm were studied. The effect of lead catalyst on agglomerate burning rates was also considered with catalyst levels up to 0.9 g Pb/kg C.

The rate of combustion of neat samples increased as the ultimate carbon particle size decreased--similar to earlier findings in this laboratory. Blending samples yielded a regular progression between the limiting values for neat samples. Maximum changes in burning rate by blending were in the range 20-40%, with the greatest changes observed at kinetic-controlled conditions. Addition of lead catalyst increased burning rates as well--by as much as a factor of two--particularly under kinetic-controlled conditions. Greatest burning rate increases were observed for catalyst levels up to 0.25 g Pb/kg C with the effect of increasing catalyst levels to higher values being relatively small.

Both theoretical and experimental results suggest that primary fuel formulation efforts should be concentrated on improving the atomization quality of carbon-black slurries as opposed to efforts to increase the fundamental reactivity of the agglomerates.

Accession For
NTIS GRA&I ☒
DTIC TAB ☐
Unannounced ☐
Justification

By
Distribution/
Availability Codes
Dist | Avail and/or Special
A-1

DTIC COPY INSPECTED 3

TABLE OF CONTENTS

TABLE OF CONTENTS (Continued)

LIST OF ILLUSTRATIONS

LIST OF ILLUSTRATIONS (Continued)

LIST OF ILLUSTRATIONS (Continued)

LIST OF TABLES

SYMBOLS

a_i - area/reactivity factor

A - cross-sectional area

C_D - drag coefficient

C_p - specific heat

d_p - agglomerate diameter

d_u - ultimate particle diameter

F - fuel-air ratio

i - enthalpy

K_v - volumetric burning rate, Eq. (21)

m - mass

$\dot{m}$ - mass flowrate

$\dot{m}'$ - mass flowrate per unit length

M_i - molecular weight of species i

n - power-law exponent

P - pressure

q_r' - radiant heat transfer per unit length

q_c'', q_r'' - convective and radiative heat flux

r - radius

R - gas constant

R_i - reaction rate of species i

Re - Reynolds number

t - time

T - temperature

V - velocity

x - axial coordinate

SYMBOLS (Continued)

x_a - length over which secondary air is injected

y - atomic hydrogen to carbon ratio

ϵ - emissivity or extent of reaction

η_c - combustion efficiency based on carbon burnout

ξ - transport enhancement factor

ρ - density

σ - Stefan-Boltzmann constant

ϕ - equivalence ratio

Subscripts

a - air

c - carbon

f - flame

g - gas or gas-phase

o - initial

OA - overall

p - particle

ref - reference

s - stoichiometric

w - wall

wb - wet bulb

1. Introduction

1.1 Background

Carbon-black slurries have received considerable attention in recent years because of their potential as high energy density (volumetric basis) liquid fuels for volume-limited propulsion systems [1].* The overall objective of this study was to investigate the combustion properties of one class of slurry fuels; namely, carbon-black slurries, in order to provide information useful for fuel and combustor development efforts.

Significant work has been devoted to the formulation of slurry fuels and their atomization, and combustion properties as sprays [2-8]. These studies have shown that combustible, high-performance slurry fuels can be formulated and burned. However, difficulties have been encountered in obtaining good combustion efficiencies indicating that carbon slurries require greater combustor residence times than conventional single-phase liquid fuels.

Earlier work in this laboratory focused on obtaining a better understanding of combustion efficiency problems with carbon-slurry fuels by studying the combustion properties of individual drops in environments representative of practical combustion chamber conditions [9-14]. The initial phases of this work considered slurry drops supported from fine quartz wires and thermocouples at various points within a turbulent diffusion flame burning in air [9-11]. It was found that slurry drop combustion was a two-stage process. The first stage involved heat-up and gasification of the liquid fuel, leaving all the slurry particles originally in the drop as a porous solid agglomerate. The second stage involved heat-up and reaction of the solid agglomerate. In general, the agglomerate reaction stage was at least an order of magnitude longer than the liquid evaporation stage; therefore, agglomerate reaction is the rate-controlling step of the carbon-slurry combustion process and the slowness of this step is the reason that larger combustor residence times are needed for good performance.

These studies also involved efforts to model the combustion lifetime (variation of drop diameter and temperature as a function of time) of slurry drops [9-11]. Predictions were evaluated by comparison with measurements obtained at various points in the flame. The liquid gasification stage was modeled using techniques developed for analysis of drops in sprays in this laboratory [15,16]. A new model of agglomerate reaction was developed utilizing a shrinking sphere model [9,10]. Two carbon reaction mechanisms were evaluated: (1) the $C/O_2/OH$ reaction mechanism of Neoh et al. [17]; and a $C/O_2/CO_2/H_2O$ mechanism which was an extension of a model used by Libby and Blake [18,19]. Reactant equilibrium at the particle surface was assumed in both cases. Empirical factors were defined to

---

*Numbers in brackets denote references.

treat the effect of pores on particle density, convective transport rates and reaction area. These factors were found to be relatively independent of flame conditions and agglomerate diameter. Using fixed values of empirical parameters, good agreement was obtained between predicted and measured drop/agglomerate properties for supported drops having initial diameters in the range 400-1000 μm [9,10].

While these findings were encouraging, questions remained concerning the extrapolation of the results to small-size particles more typical of practical sprays. This motivated a second stage of the investigation where freely moving particles were studied in the post-flame region of a flat-flame burner [11-14]. Since the liquid gasification stage was relatively straightforward, only dried agglomerates were studied. Measurements provided the variation of particle size, mass and temperature as a function of time for particles having initial diameters in the range 10-100 μm. These results yielded more complete information concerning the empirical factors used in the analysis. It was found that empirical parameters varied with extent of reaction but were relatively independent of particle size and flame conditions. Some limited tests were completed with carbon slurries containing blends of carbon-black particles having different ultimate carbon particle sizes. The results indicated that blends tended to burn somewhat slower than agglomerates of either constituent--although the effect was not large. This was attributed to the smaller particles inhibiting the development of pores.

The agglomerate combustion model was evaluted using the new data for small freely-moving agglomerates [11-14]. Using simple correlations of empirical parameters as a function of extent of reaction and agglomerate type, good agreement was obtained between predicted and measured particle properties. A significant finding was that the new values of the empirical parameters were approximately the same as those found during the earlier studies with large supported particles over much of the lifetime of the agglomerates.

In summary, the earlier fundamental studies [9-14] established methods for predicting the combustion lifetime of carbon-black slurry drops for a relatively wide range of conditions in environments typical of combustion chambers. This included several carbon-black formulations, initial drop sizes of 10-1000 μm, local fuel equivalence ratios of 0.2-1.4, and local temperatures of 800-1950K--all at atmospheric pressure.

1.2 Objectives

The purpose of the present investigation was to extend the earlier results with two major objectives. The first was to apply the slurry drop combustion model to a one-dimensional analysis of a slurry-fueled combustor. The resulting model was used for a parametric investigation of combustion chamber characteristics--

seeking guidelines for practical combustion chamber design. Parameters considered included initial carbon agglomerate size, chamber pressure, secondary air schedule, mass loading, initial agglomerate temperature, initial slip velocity, and slurry properties.

The second objective was to extend the data base of agglomerate combustion properties. The earlier measurements considered neat slurries (monodisperse ultimate carbon particle sizes) and a single bimodal blend consisting of equal parts (by mass) of carbon blacks having ultimate carbon particle sizes of 70 and 350 nm [9-14]. Limited information had also been obtained concerning effects of catalyst [9,10]. The new tests considered additional blends, as well as effects of catalyst. These tests were conducted using agglomerate particles supported in the post-flame region of a flat-flame burner. Partially reacted agglomerates were also observed with a scanning electron microscope (SEM)--to help interpret burning rates in terms of surface morphology.

Results from both aspects of the investigation are reported in the following. The report begins with a description of the one-dimensional combustor analysis and its results. This is followed by a description of the new supported particle tests and the results of these experiments.

2. Combustor Model

2.1 Basic Assumptions

In the following, a carbon-black slurry combustor is modeled as a one-dimensional flow consisting of a dilute mixture of agglomerate particles and products of combustion. This implies that the volume occupied by the agglomerate particles is negligible. With this approach, it was assumed that the relatively slow burning carbon agglomerates survive the primary combustion zone (where the liquid fuel is burned) and subsequently burn out in the secondary zone. Mixing rates of the secondary air, the particle products of combustion and the bulk gas are assumed to be infinitely fast. Particle combustion rates are determined using the extended Libby and Blake mechanism for the reaction of carbon with O_2, CO_2 and H_2O with the assumption of equilibrium reactant concentrations of the particle surface [9]. Initial gas-phase conditions are determined by assuming adiabatic combustion of the liquid fuel component (JP-10) without any combustion of solid carbon in a primary zone.

2.2 Mass Conservation

Considering the control volume shown in Fig. 1, the change of gas-phase mass flow rate with distance is

$$d\dot{m}_g/dx = - d\dot{m}_c/dx + \dot{m}_a' \tag{1}$$

The solid-phase carbon flow rate can be expressed in terms of the initial solid carbon flow rate and the local and initial particle radius and density

$$\dot{m}_c = \dot{m}_{c,o}(\rho_p/\rho_{p,o})(r_p/r_{p,o})^3. \tag{2}$$

Differentiating Eq. (2) yields the rate of change of solid carbon with distance,

$$d\dot{m}_c/dx = (3\rho_p r_p^2/\rho_{p,o} r_{p,o}^3) dr_p/dx + (r_p^3/r_{p,o}^3 \rho_{p,o})\, d\rho_p/dx. \tag{3}$$

To calculate the particle radius history, the agglomerate reaction theory of Szekely and Faeth [9] was employed. Boundary conditions for this analysis were determined by assuming equilibrium in the gas-phase. The rate of change of particle radius with distance can be expressed as follows [13]

$$dr_p/dx = - \sum_i a_i R_i/\rho_p\, V_p \tag{4}$$

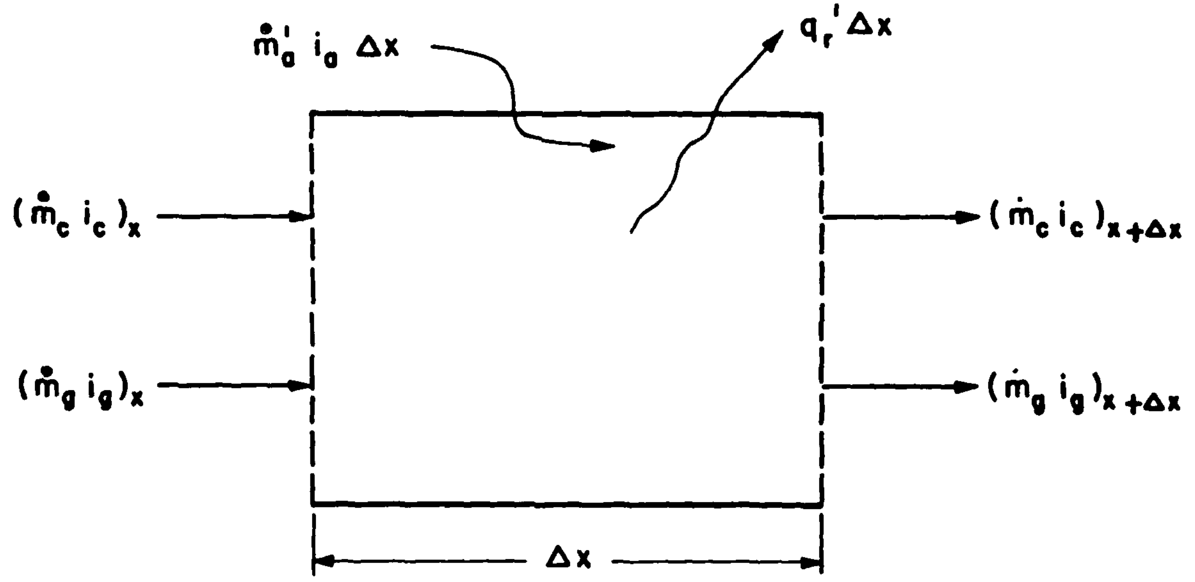

Fig. 1. Elemental control volume used for one-dimensional formulation.

where i represents O_2, CO_2 and H_2O. The following correlations for particle density, ρ_p, transport enhancement factor, and area/reactivity factors, a_i, were employed [12]:

$$\rho_p = \rho_{p,o} (1-\varepsilon)^{0.6} \tag{5a}$$

$$\xi = 1.49 - 0.01716\, r_{po} + 18.3\, \varepsilon - 13.2\, \varepsilon^2 - 1.77\, d_u \tag{5b}$$

$$a_{O2} = 61.3 - 0.412\, r_{po} + 23.7\, \varepsilon + 2.27/d_u \tag{5c}$$

$$a_{CO_2} = 109.6 - 0.580\, r_{po} + 43.2\, \varepsilon + 5.56/d_u \tag{5d}$$

$$a_{H_2O} = 164.7 - 1.026\, r_{po} + 50.1\, \varepsilon + 4.21/d_u \tag{5e}$$

where r_{po} and d_u have the units µm.

The gas-phase composition was determined from the following mass balances combined with the equilibrium assumption:

$$\dot{m}_{c,g} = (\dot{m}_{c,g})_o + \dot{m}_{c,o}[1-(\rho_p/\rho_{p,o})(r_p/r_{p,o})^3] \tag{6a}$$

$$\dot{m}_a = \dot{m}_{a,o} + \int_o^x \dot{m}'_a \, dx \tag{6b}$$

$$\dot{m}_{H_2} = (\dot{m}_{H_2})_o \tag{6c}$$

Equations (6a-6c) were used to determine the apparent gas-phase hydrogen-carbon ratio, the local fuel-air ratio, and stoichiometric fuel-air ratio which in turn are used to define the local gas-phase equivalence ratio. The equivalence ratio then can be expressed as

$$\phi = (\dot{m}_{c,g} + \dot{m}_{H_2})/\dot{m}_a F_s \tag{7}$$

where

$$F_s = \frac{M_c + yM_H}{4.764\, M_a\, (1 + y/4)} \tag{8}$$

with

$$y = \dot{m}_{H_2} M_c/\dot{m}_{c,g} M_H \tag{9}$$

Assuming ideal gas behavior, the local gas velocity was computed from

$$V_g = (\dot{m}_{c,g} + \dot{m}_a + \dot{m}_{H_2})\, RT_g/PA \tag{10}$$

2.3 Energy Conservation

Referring to the control volume of Fig. 1, an overall energy balance for the combined solid and gaseous phases yields

$$\frac{d(\dot{m}_g\, i_g)}{dx} = -\frac{d(\dot{m}_c i_c)}{dx} + \dot{m}'_a\, i_a - q'_r \tag{11}$$

where the only heat loss from the flow is assumed to be due to radiation from the particles to the walls. The enthalpy change of the solid phase can be expressed as

$$\frac{d(\dot{m}_c i_c)}{dx} = \dot{m}_c\, C_{p,c} \frac{dT_p}{dx} + i_c \frac{d\dot{m}_c}{dx} \tag{12}$$

and the radiation loss is given by

$$q'_r = 4\pi\, \dot{m}_{c,o}\, \varepsilon\sigma\, r_p^2 (T_p^{\ 4} - T_w^{\ 4})/m_{p,o}\, V_p \tag{13}$$

The gas-phase temperature was calculated as follows. For constant pressure combustion the gas specific enthalpy is a function of T_g and ϕ_g only; thus,

$$di_g/dx = (\partial i_g/\partial T_g)dT_g/dx + (\partial i_g/\partial \phi_g)d\phi_g/dx \tag{14}$$

Expanding the left-hand side of Eq. (11), substituting Eq. (14) and solving for the gas temperature yields

$$\frac{dT_g}{dx} = \left\{ \frac{1}{\dot{m}_g} \left[\frac{d(\dot{m}_g\, i_g)}{dx} - i_g \frac{d\dot{m}_g}{dx} \right] - \frac{\partial\, i_g}{\partial\, \phi_g} \frac{d\phi_g}{dx} \right\} \Big/ \frac{\partial\, i_g}{\partial\, T_g} \tag{15}$$

The enthalpy partial derivatives were calculated using the simplified equilibrium routine of Olikara and Borman [20,21]. To calculate $d\phi_g/dx$ it was necessary to take into account both the changing local and stoichiometric fuel-air ratios; thus,

$$d\phi_g/dx = (dF/dx)/F_s - F(dF_s/dx)/F_s^2 \quad (16a)$$

where

$$dF/dx = (d\dot{m}_{c,g}/dx)/\dot{m}_a - \dot{m}'_a(\dot{m}_{c,g} + \dot{m}_{H_2})/\dot{m}_a^2 \quad (16b)$$

and

$$dF_s/dx = 4(dy/dx)\left[\frac{M_H}{4+y}\left(1 - \frac{y}{4+y}\right) - M_c\left(\frac{1}{4+y}\right)^2\right]/4.764\ M_a \quad (16c)$$

with

$$dy/dx = -\ \dot{m}_{H_2}\ M_c(d\dot{m}_c/dx)/M_H\dot{m}_c^2 \quad (16c)$$

As given in [9], conservation of energy for a particle having uniform temperature yields:

$$dT_p/dx = -\ 3\left[\sum_i a_i R_i(i_p - i_c) + q''_c + q''_r\right]/\rho_c C_{p,c} r_p V_p \quad (17)$$

2.4 Momentum Conservation

For the gas-phase, momentum conservation is trivial since it was assumed that pressure gradients were negligible. For a single particle, the only force assumed to be important was the drag force. Particle momentum conservation then yields

$$dV_p/dx = -\ 3C_D\rho_g(V_p - V_g)\left|V_p - V_g\right|/8\rho_p r_p V_p \quad (18a)$$

where the drag coefficient was expressed as [22]:

$$C_D = 24/Re + 6/(1 + Re^{1/2}) + 0.4 \quad (18b)$$

To complete the model, the transit time for a particle emerging from the primary zone to reach any downstream location was obtained by integrating

$$dt/dx = 1/V_p \tag{19}$$

2.5 Solution Technique

After specifying appropriate initial conditions, the set of 5 coupled ordinary differential equations (Eqs. (4), (15), (17), (18a) and (19)) was integrated using a fourth-order Adams predictor-corrector method. This solution provided local values for unburned carbon fraction, gas-phase and solid-phase temperatures, gas and particle velocities, and gas-phase composition.

3. Parametric Investigation

3.1 Parameter Identification

To provide guidelines for combustor design, the influence of carbon agglomerate diameter, chamber pressure, secondary air scheduling, and non-dimensional reference velocity (or mass loading) on combustor performance were evaluated using the model developed above. Additionally, the effects of agglomerate slip velocity and degree of agglomerate preheat upon emerging from the primary zone were evaluated, since these parameters appear in the model as unknown initial conditions. Three or more levels of these six parameters were chosen to be representative of the likely range of values. These parameters are shown in Table 1 with the central value used as the "standard" value. Calculations were carried out with all but one parameter fixed at the standard level, except as noted. Also the effect of catalyst addition [13] and ultimate particle diameter were investigated at two levels.

Interaction of the above parameters with the primary zone parameters was ignored. Thus, for example, the effect of chamber pressure on the primary zone flame temperature was neglected to isolate the effects of pressure in the secondary zone. Values for fixed parameters are given in Table 2.

3.2 Results and Discussion

3.2.1 Typical Life History

Figure 2 is an illustration of a typical history of an agglomerate particle as it moves downstream through the changing combustor environment. The downstream distance has been normalized by the length over which secondary air is injected. This length was chosen such that approximately 98% of the solid carbon was consumed by the end of air addition for the standard set of parameters. From the figure, it can be seen that the initial burning rate is quite slow until the particle heats to about 1500-1700K. This is followed by a relatively rapid burning up to an x/x_a of about 0.25, after which the burning rate begins to decrease. From this behavior, it appears that diffusion-controlled burning dominates the carbon burnout process. The initial gas-phase equivalence ratio is controlled principally by secondary air addition until the carbon combustion rate accelerates sufficiently at x/x_a of approximately 0.08. The gas velocity monotonically increases as additional mass enters the gas-phase from both secondary air injection and carbon combustion. With the specified initial slip velocity, the agglomerate particle slows down to zero slip at approximately $x/x_a \approx 0.10$, and thereafter, the particle is accelerated by the gas phase.

In the following sections, the effects of the combustor parameters given in Table 1 on combustor performance are presented and discussed.

Table 1. Variable Combustor Parameters

Condition	Level		
	Low	Standard	High
Agglomerate particle diameter (μm)	10	25	50,75,100
Chamber pressure (atm)	1	10	20
Secondary air schedule[a]	--	--	--
Non-dimensional reference velocity[b]	0.5	1.0	2.0
Initial particle slip ratio, $V_{p,o}/V_{ref}$	1.0	1.5	2.0
Initial particle preheat, $(T_{p,o}-T_{wb})/(T_f-T_{wb})$	0	0.25	0.50
Catalyst addition	--	no	yes
Ultimate particle size (nm)	70	300	--

[a] The standard secondary air schedule consisted of a constant air injection rate per unit length m_a' up to a non-dimensional length of 1.0. A ramp schedule was a linear distribution decreasing to zero at a non-dimensional length of 1.0. The spike schedule was a constant m_a' up to a non-dimensional length of 0.10.

[b] Reference velocity as used herein is defined as the velocity of the gas emerging from the primary zone prior to addition of secondary air.

Table 2. Fixed Combustor Parameters

Primary zone flame temperature, T_f	-	2380K
Secondary air temperature, T_a	-	700K
Solid carbon weight loading	-	56%
Primary zone equivalence ratio, ϕ_O	-	1.0
Overall equivalence ratio, ϕ_{OA}	-	0.30
Ultimate particle diameter, d_u	-	300 nm
Non-dimensional length of secondary air injection zone	-	1.0

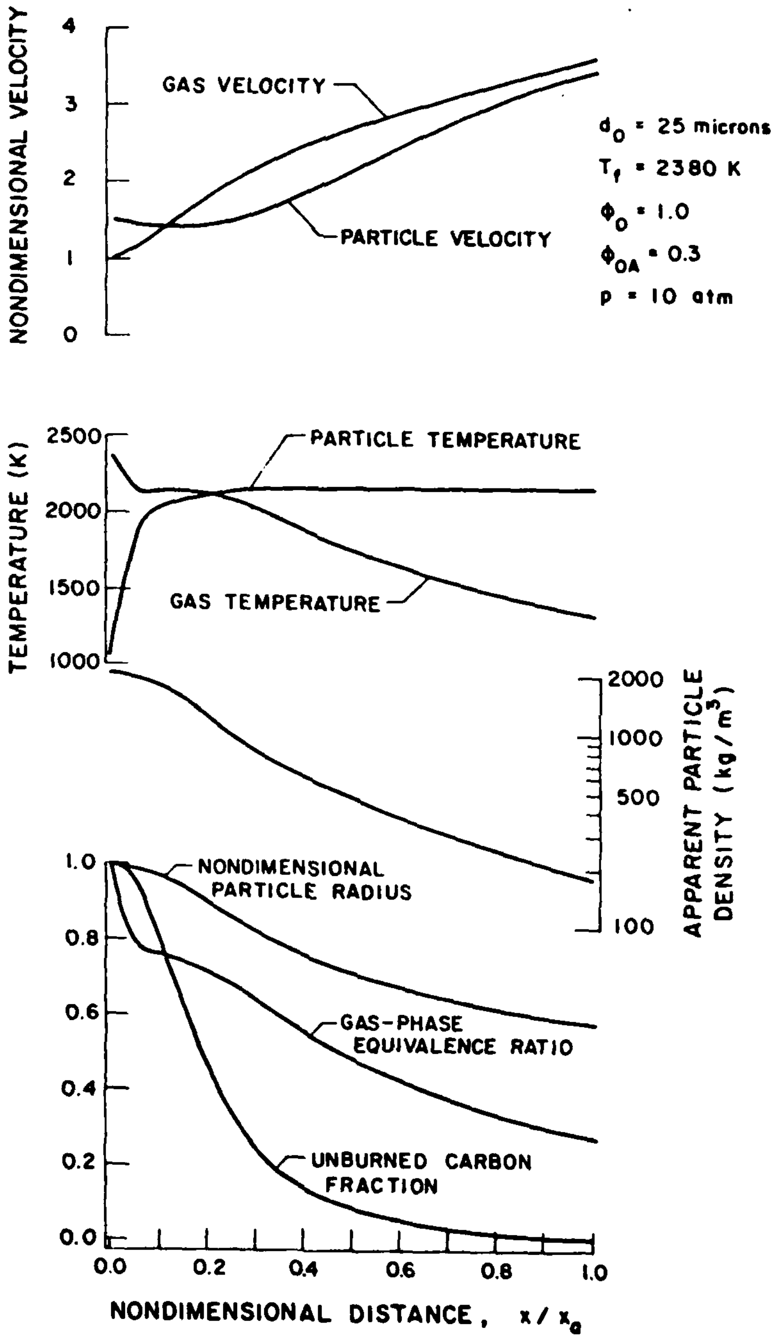

Fig. 2. Agglomerate particle life history and combustor environment.

3.2.2 Particle Diameter

Figure 3 shows the unburned carbon fraction as a function of distance through the secondary zone. The termination of each curve represents approximately 98% complete carbon combustion. The effect of initial particle diameter is quite marked with the length required for 98% combustion efficiency increasing more than an order of magnitude for particle sizes increasing from 10 to 100 µm. This result is not unexpected since individual particle burning rates, $d(d_p)/dt$, are roughly inversely proportional to particle diameter at the high-temperature or diffusion-control limit [9]. For the range of particle diameters and conditions selected, diffusion-controlled combustion appears to dominate the carbon burnout process. To quantify the influence of agglomerate diameter--as well as the other parameters investigated--exponents for a power-law type dependence of burning time on parameter variation were calculated for various extents of reaction, ε, i.e.,

$$(t_1/t_2)_{\varepsilon = \text{const.}} = (P_1/P_2)^n \tag{20}$$

where P is any of the parameters investigated. Table 3 provides the exponents, n, for $\varepsilon = 0.05$, 0.5 and 0.95 for five parameters. From Table 3 it can be seen that the particle size effect is relatively independent of extent of reaction with an average exponent of 1.32. For kinetic-controlled combustion, an exponent of 1.0 would be expected, while an exponent of 1.5-2.0 is predicted by a simple diffusion-controlled analysis. The calculated value of 1.32 indicates that diffusion plays a somewhat greater role in limiting reaction rates than does chemical kinetics. The strong influence of initial agglomerate size suggests a well-atomized spray is most beneficial for efficient combustion in a limited-length combustor.

Particle temperature and gas temperature are shown as functions of downstream distance in Figs. 4 and 5, respectively. Note that the abscissa of these figures has been expanded to show the heat-up period in more detail. For the lifetime of the 10 µm particle the gas temperature always exceeds the particle temperature because of the rapid heat release with small particles. The temperature of the larger particles, however, after an initial heat-up period exceeds the gas temperature, and the particles lose heat to the surroundings by both convection and radiation.

Dimensionless particle velocity through the combustor is shown in Fig. 6. Also shown is the gas velocity for the 10 µm and 100 µm limit cases. For the 10 µm case, it can be observed that the particle slip velocity is relatively small over the particle lifetime in comparison to the 100 µm case. Thus, a more favorable environment for convective transport exists for the larger particles--enhancing the diffusion rates of oxidant to the particle surface, and conversely, increasing the convective heat loss.

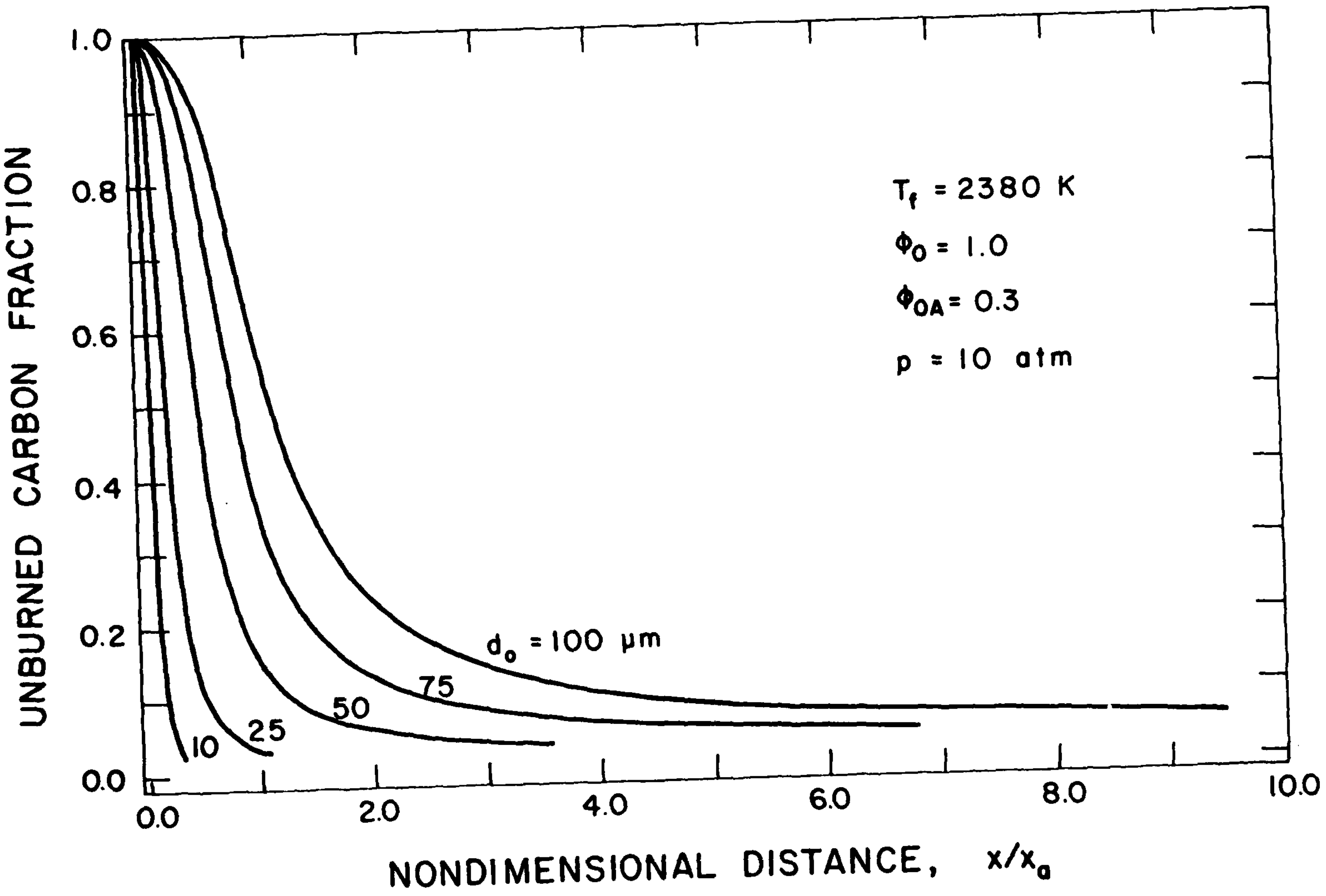

Fig. 3. Unburned carbon fraction versus non-dimensional distance for initial agglomerate diameters ranging from 10 to 100 μm.

Table 3. Burning Time Power-Law Exponents

Parameter	ε = 5%	ε = 50%	ε = 95%
Agglomerate particle diameter	1.32	1.26	1.39
Chamber pressure	-0.192	-0.153	-0.156
Reference velocity, fixed air injection length	-0.268	-0.324	-0.414
Reference velocity, scaled air injection length	-0.144	-0.084	-0.091
Initial particle slip ratio	-0.573	-0.271	-.115
Initial particle temperature ratio, $T_{p,o}/T_f$	-0.805	-0.174	-0.006

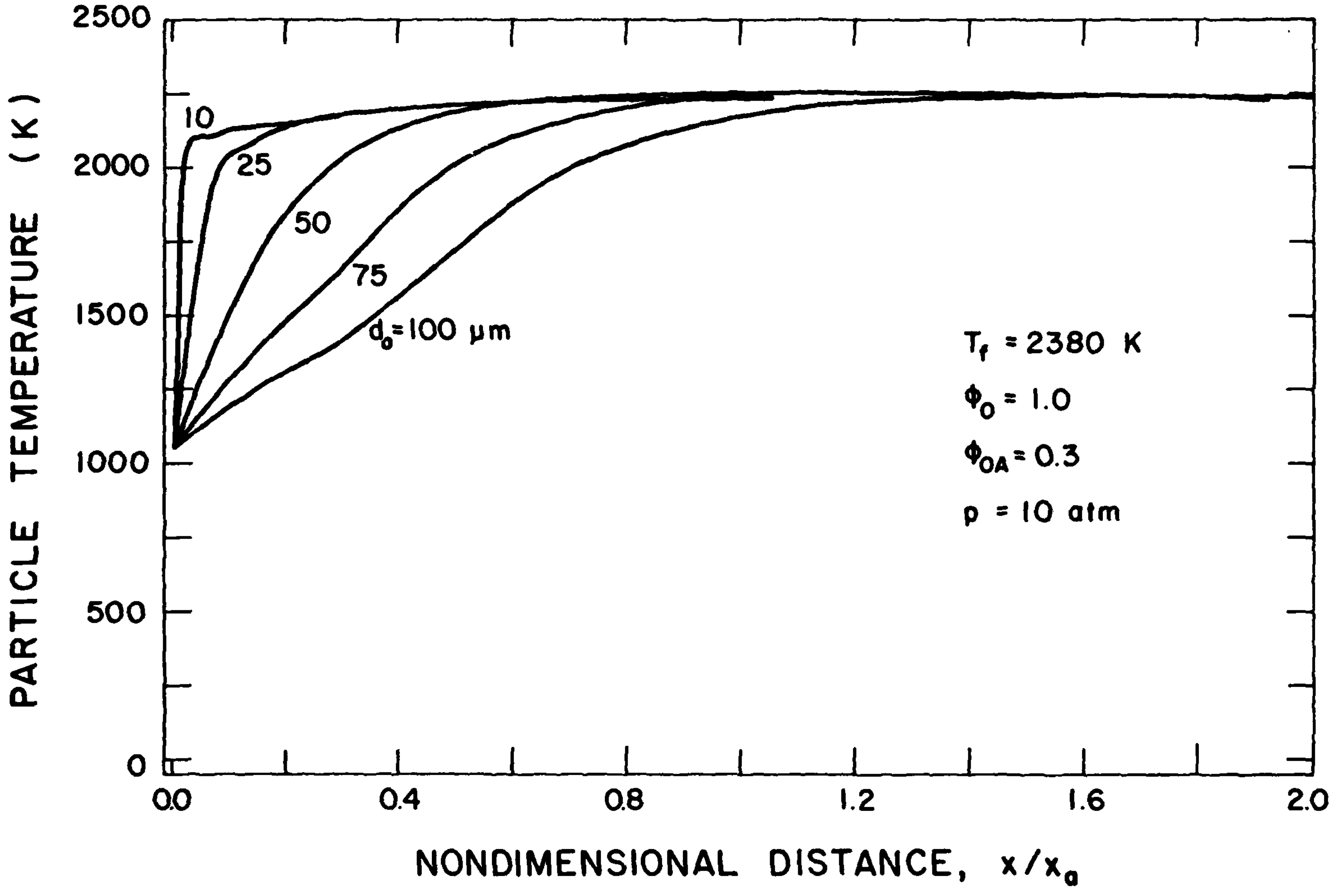

Fig. 4. *Particle temperature versus non-dimensional distance for initial agglomerate diameters ranging from 10 to 100 μm.*

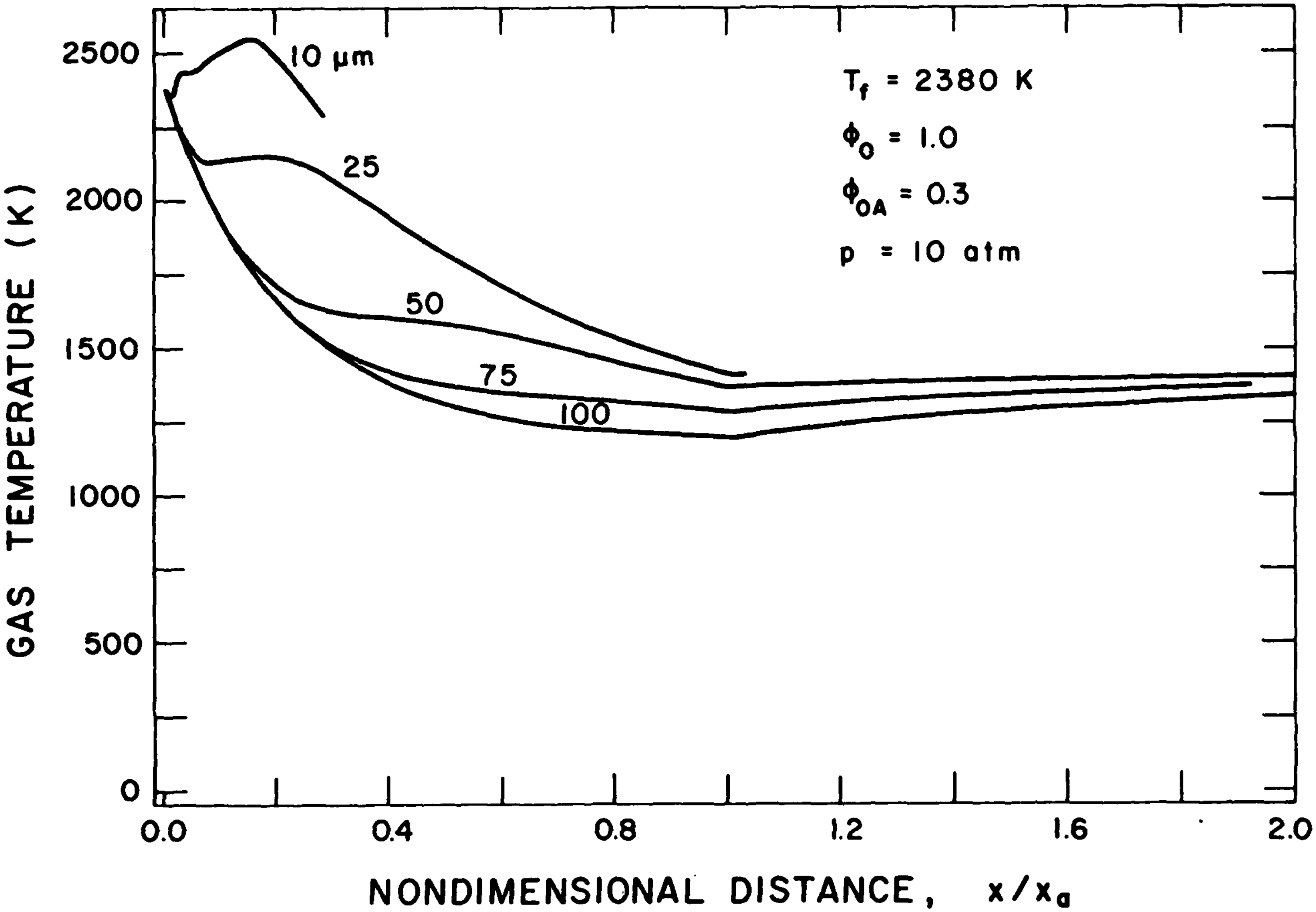

Fig. 5. Gas temperature versus non-dimensional distance for initial agglomerate diameters ranging from 10 to 100 μm.

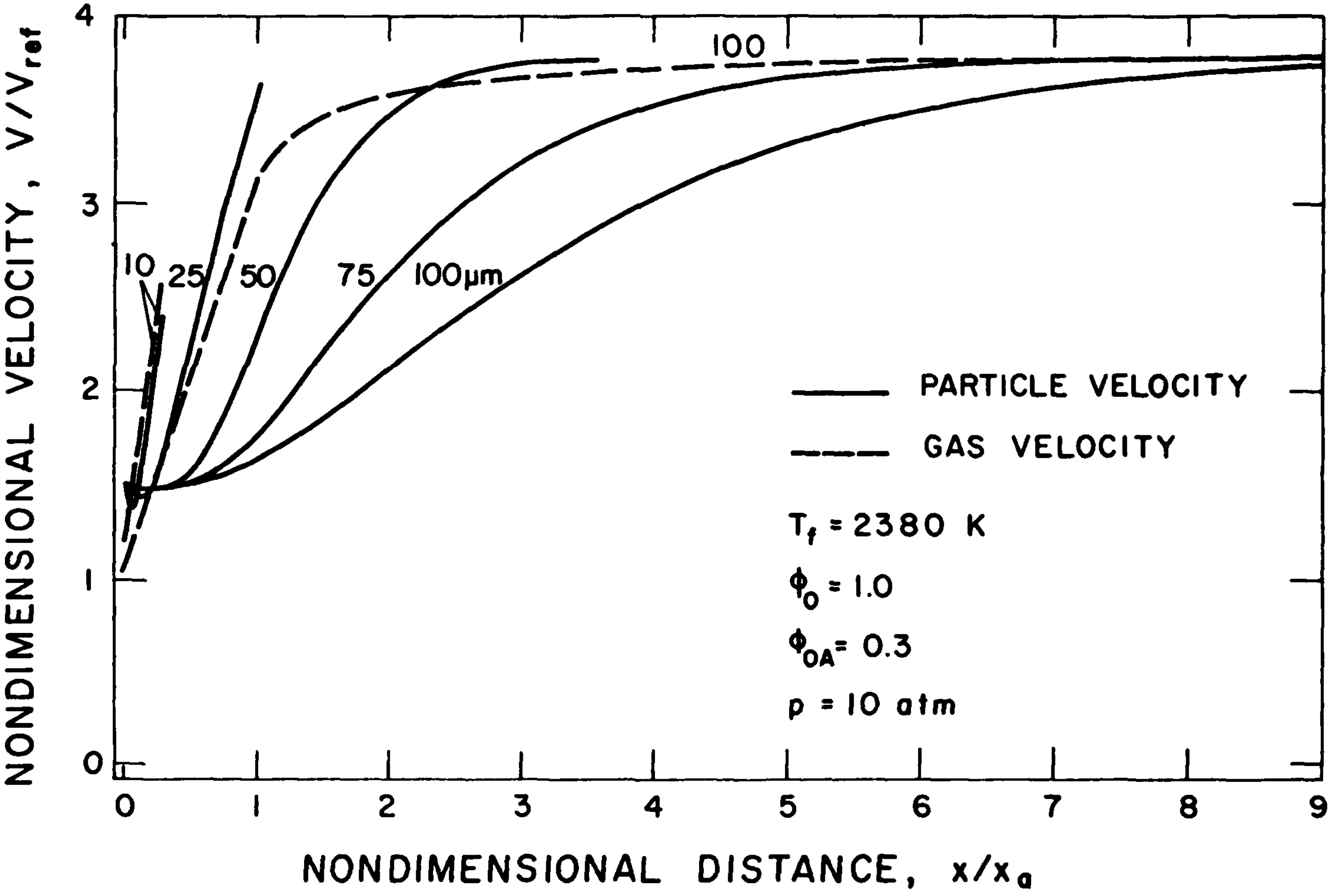

Fig. 6. Non-dimensional particle and gas velocities versus non-dimensional distance for various initial agglomerate diameters.

3.2.3 Chamber Pressure

A change in chamber pressure from 1.0 to 20 atm results in significantly increased burning rates and shortened combustor lengths to achieve $\eta_c = 98\%$ as shown in Fig. 7. Again, the power-law exponent for burning time dependence on pressure (Table 3) is only a weak function of extent of reaction with an average value of $n = -0.167$. Pressure effects manifest themselves principally through the concentration of reactants at the particle surface and shifting of gas-phase equilibrium.

3.2.4 Secondary Air Schedule

Three different secondary air schedules, as illustrated in Fig. 8, were evaluated. The standard schedule consisted of a constant air injection rate per unit length up to a non-dimensional length of unity. To achieve earlier air introduction, a ramp and "spike" distribution were applied. The ramp schedule was a linear distribution decreasing to zero at $x/x_a = 1.0$, while the spike was a constant rate per unit length over 1/10 of the standard length.

Figure 9 illustrates the importance of the manner in which air is added into the secondary combustion zone by comparing the effect of the three secondary air schedules. From the figure it can be seen that the earlier the air is introduced, the greater the carbon burnout in a fixed length. This effect is most pronounced at combustion efficiencies less than 98%. At the 98% level, the combustor length required varies only a few percent among the air injection schedules, while at the 90% level, combustor lengths differ 30% between the standard and "spike" air schedule. Two consequences of the early air introduction work together to enhance the agglomerate combustion; first, the production of an oxidizer-rich environment during the early stages of combustion, and, secondly, the greater slip velocity enhancing the mass transport rates. Gas temperatures are shown in Fig. 10. The rapid air introduction of the spike schedule causes the gas temperature to initially fall rapidly and achieve a minimum at the termination of air injection. At this same location, a minimum gas-phase equivalence ratio of 0.21 is reached. During the spike injection, $0 < x/x_a < 0.1$, particle slip velocities generally exceed those for the standard schedule seen in Fig. 11. Thus, transport coefficients for both heat and mass are enhanced by spike injection. It follows then that mass transfer rates should be greater for the spike case since both the driving potential and the transport coefficient exceed those of the standard schedule; however, for heat transfer the rapid air introduction decreases the driving potential $(T_g - T_p)$ during the heat-up period resulting in slightly lower particle temperatures as seen in Fig. 12. Once combustion is well under way, particle temperatures for the spike injection then exceed those of the other two schedules. As the agglomerate particles move downstream, the effects of increased slip and increased free stream oxidant concentration diminish, resulting in nearly the same length of combustor as carbon combustion efficiencies approach 100%.

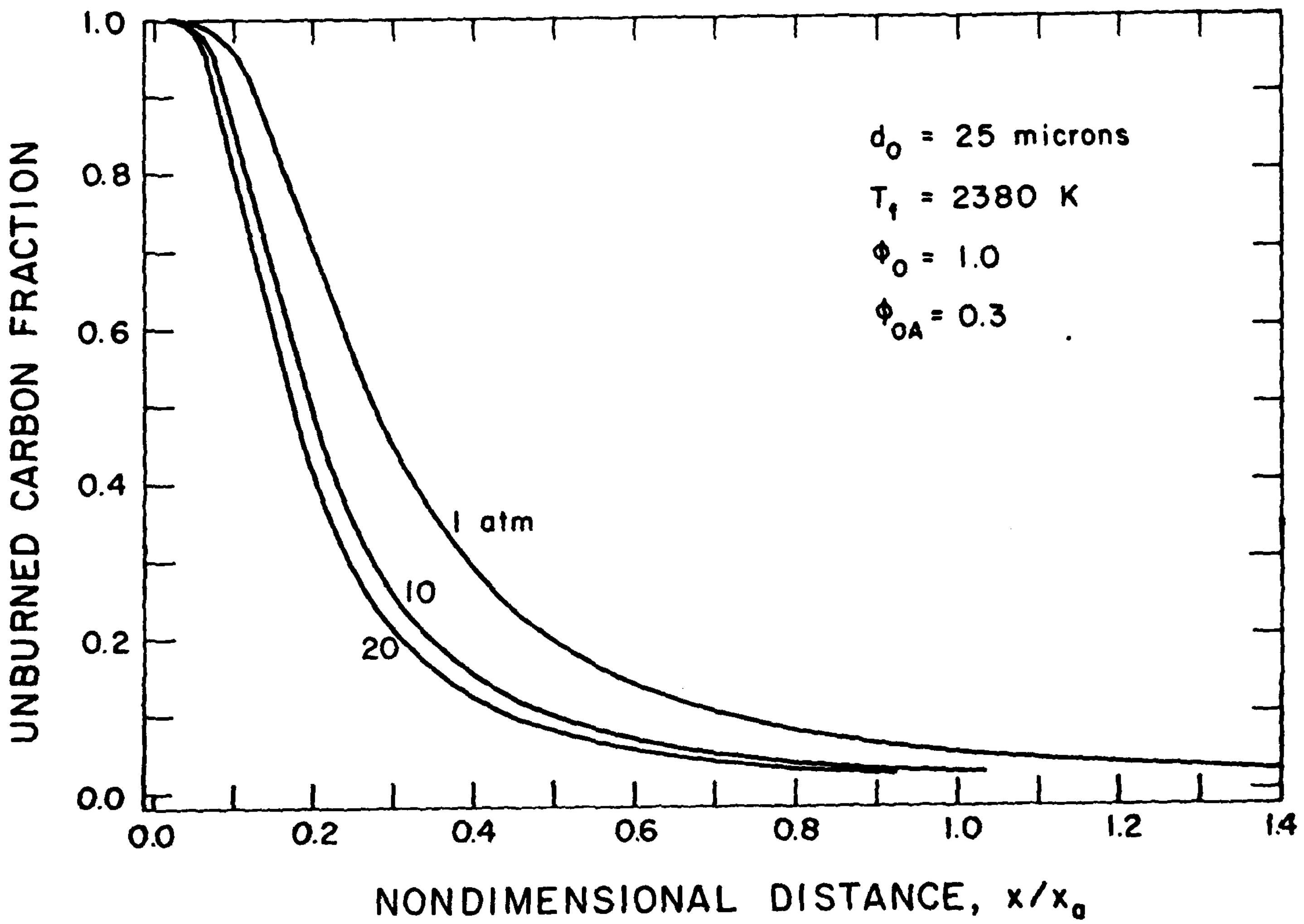

Fig. 7. Unburned carbon fraction versus non-dimensional distance for chamber pressures of 1, 10 and 20 atm.

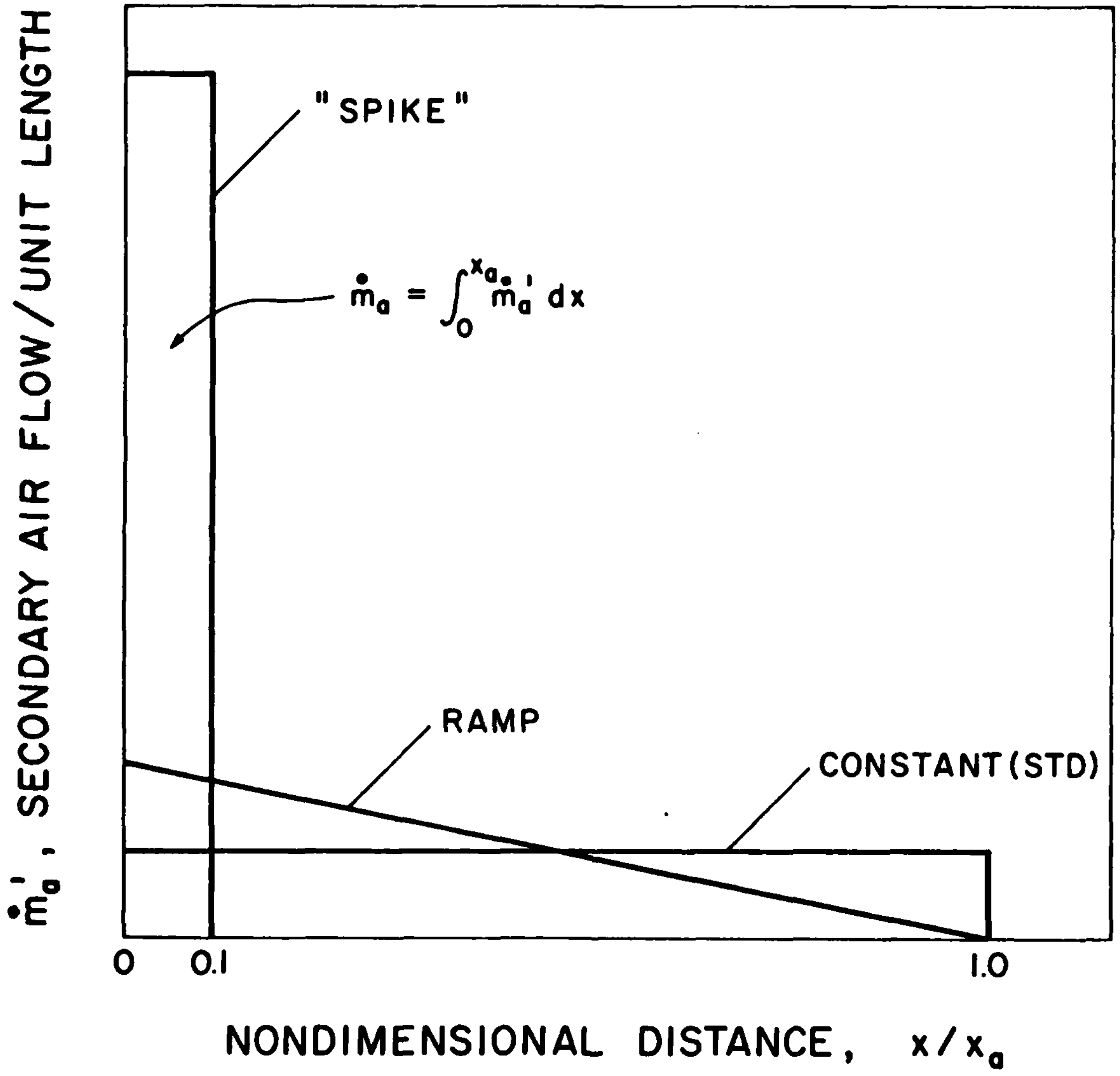

Fig. 8. Secondary air schedules.

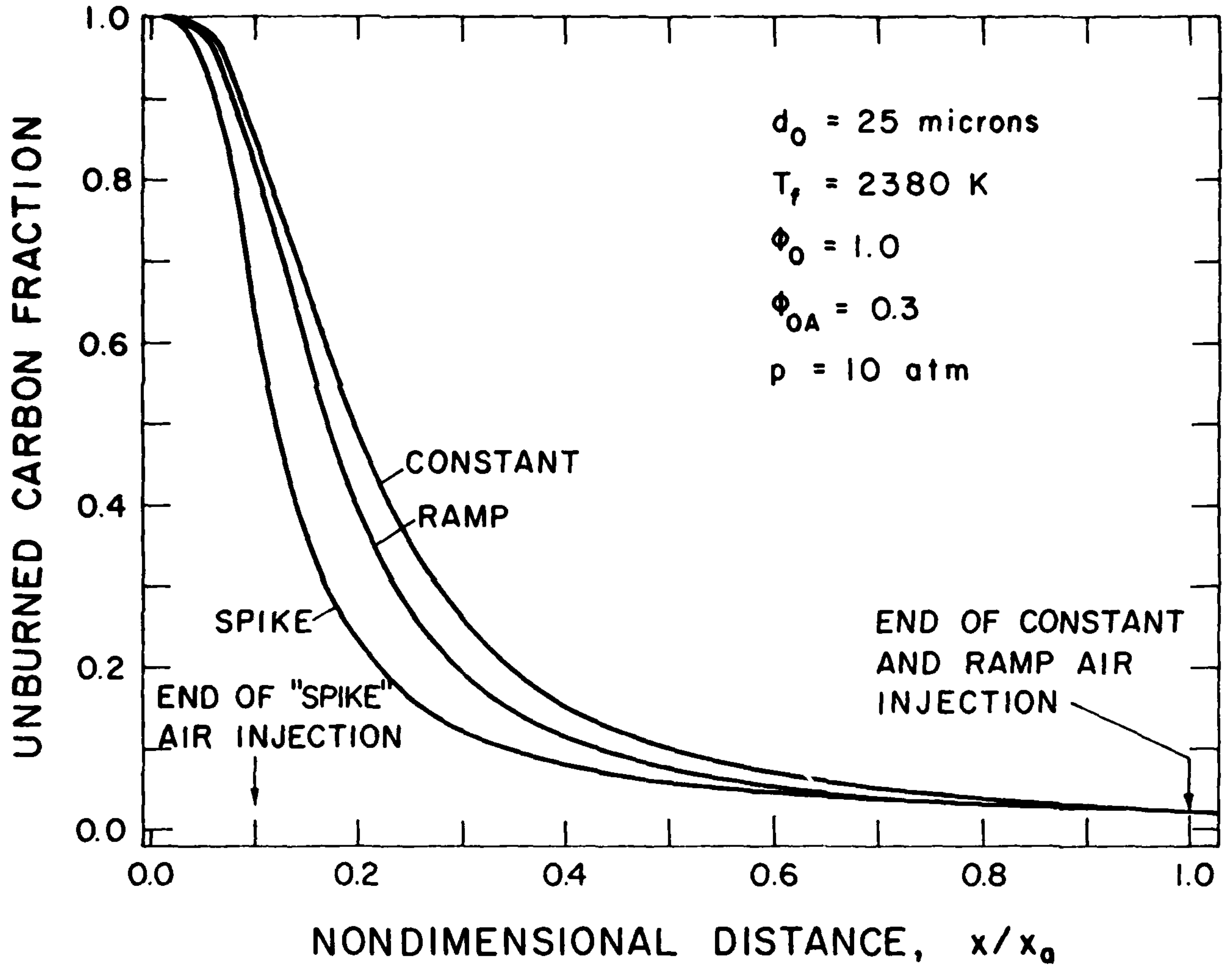

Fig. 9. Unburned carbon fraction versus non-dimensional distance for three different secondary air schedules.

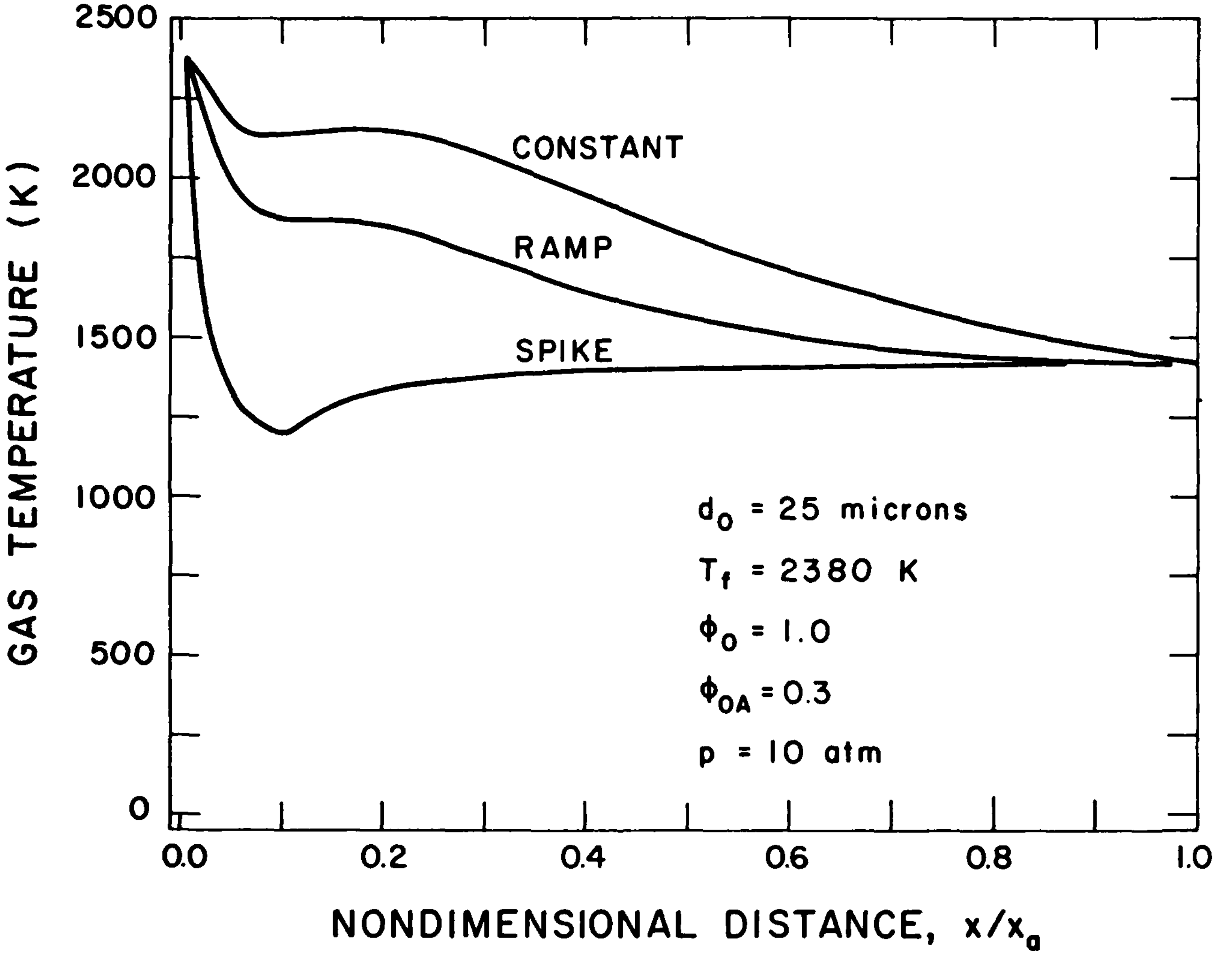

Fig. 10. Gas temperature versus non-dimensional distance for various secondary air schedules.

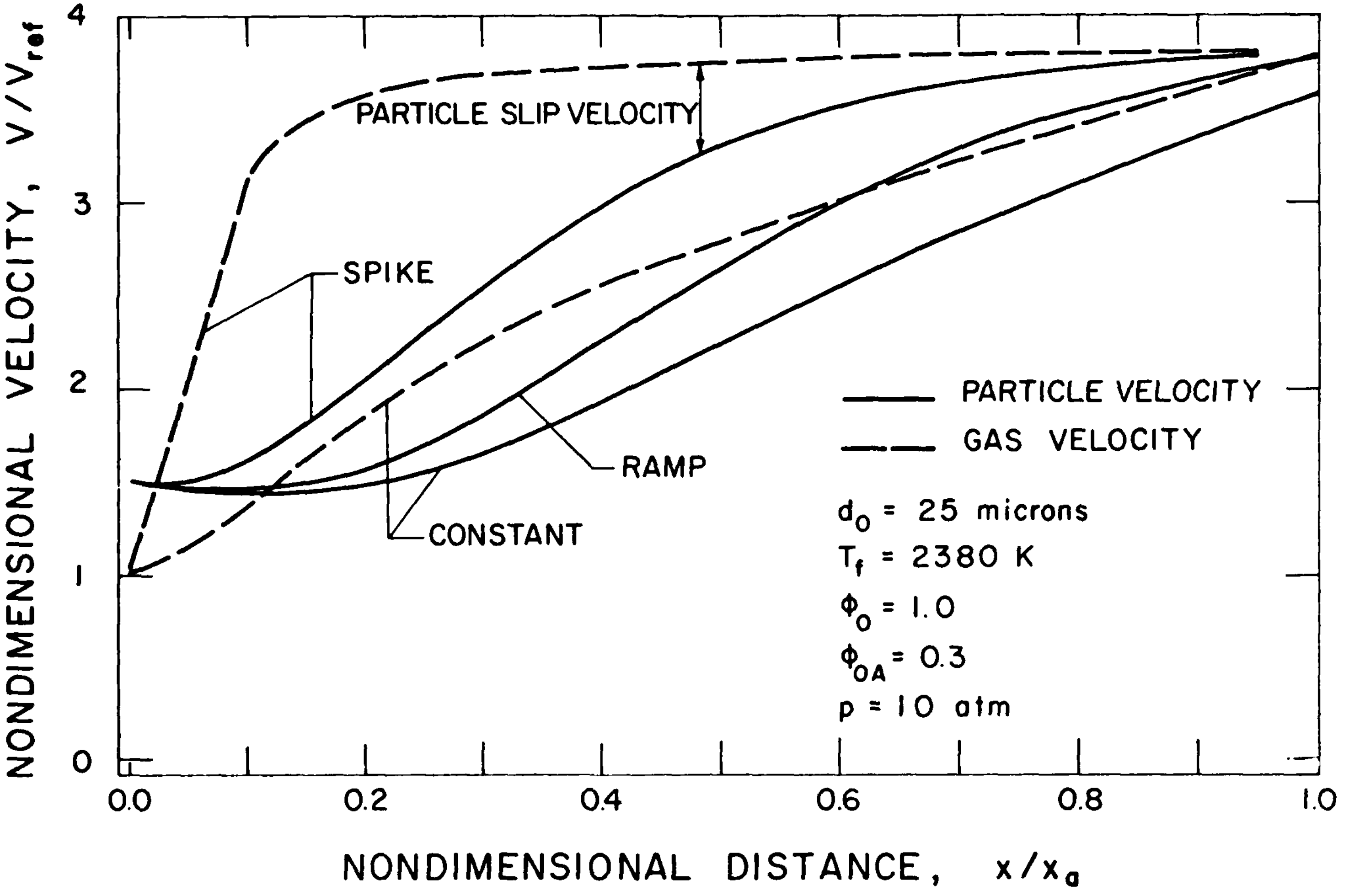

Fig. 11. Dimensionless particle and gas-phase velocities versus distance for various secondary air schedules.

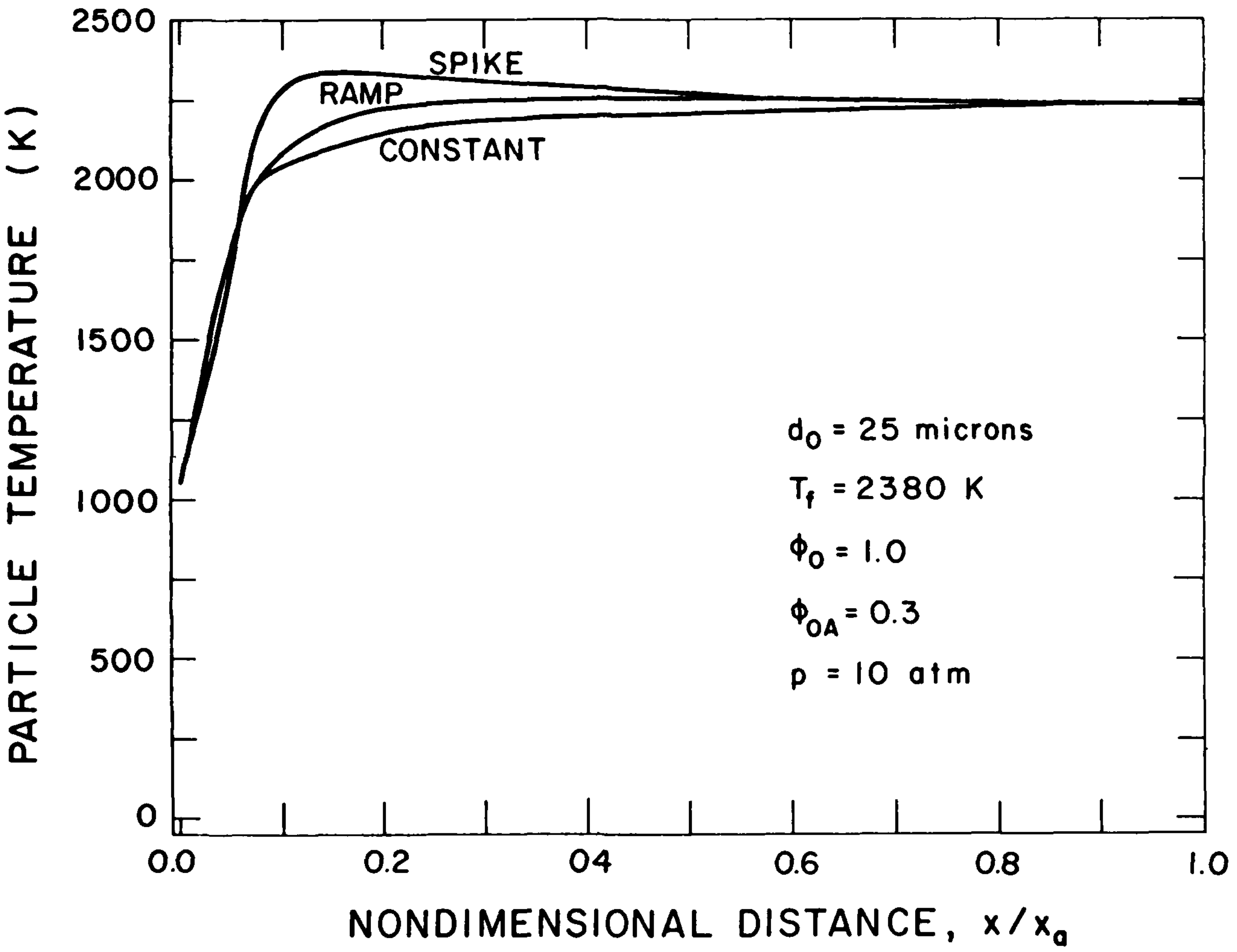

Fig. 12. Particle temperature versus non-dimensional distance for various secondary air schedules.

3.2.5 Reference Velocity

The effect of dimensionless combustor reference velocity, or mass loading, on carbon burnout is shown in Fig. 13. The solid curves represent the cases where only the reference velocity was varied and the air injection length was fixed at x/x_a = 1.0. For the dashed lines, the air injection length was scaled with the reference velocity to provide approximate time-similarity so that approximately the same oxidation environment existed at the same time for all three reference velocities. In both cases, an increasing reference velocity requires a greater combustor length for the same combustion efficiency, as one would expect based on residence time considerations alone. Table 3 also shows that burning times decrease with reference velocity, although only a slight dependence is seen for the scaled air injection length. Thus, the major contribution of reference velocity to enhanced combustion in the fixed air length case is the greater availability of oxygen, with enhanced transport playing a relatively minor role.

3.2.6 Initial Slip Ratio

Figure 14 is an illustration of the effect of initial particle slip velocity on carbon burnout. One can see that the lower the initial slip velocity, the shorter the distance required to achieve any given degree of carbon burnout. The principal mechanism causing the less favorable burnout at higher slip ratios is the decreased residence time in a fixed length of combustor. The time to achieve a combustion efficiency of 98% was essentially the same for all three initial slip ratios, as can be seen in Fig. 15 where unburned carbon fraction is shown as a function of time. Table 3 quantifies the diminishing effect of slip ratio on burnout time as the combustion efficiency or extent of reaction increases. The enhanced burnout in the earlier stages of reaction results from increased oxygen availability at any given time for the faster traveling, high-slip particle, as can be inferred from the plot of gas-phase equivalence ratio versus time (Fig. 16). The higher particle velocity thus produces an effect similar to early air introduction.

3.2.7 Initial Preheat

Particle temperature history is shown in Fig. 17 where particles enter the secondary zone with initial temperatures ranging from the wet-bulb temperature of liquid combustion to approximately 1500K. After an initial heat-up period--requiring a length of about 0.2--the particle temperature converges to a single line. The net effect being that initial particle preheat has little influence on either burnout length (Fig. 18) or burnout time (Table 3) for combustion efficiencies of practical importance. These results suggest that an improved combustor model should allow for a distribution of initial particle velocities, while particle preheating effects may not have to be treated in as much detail.

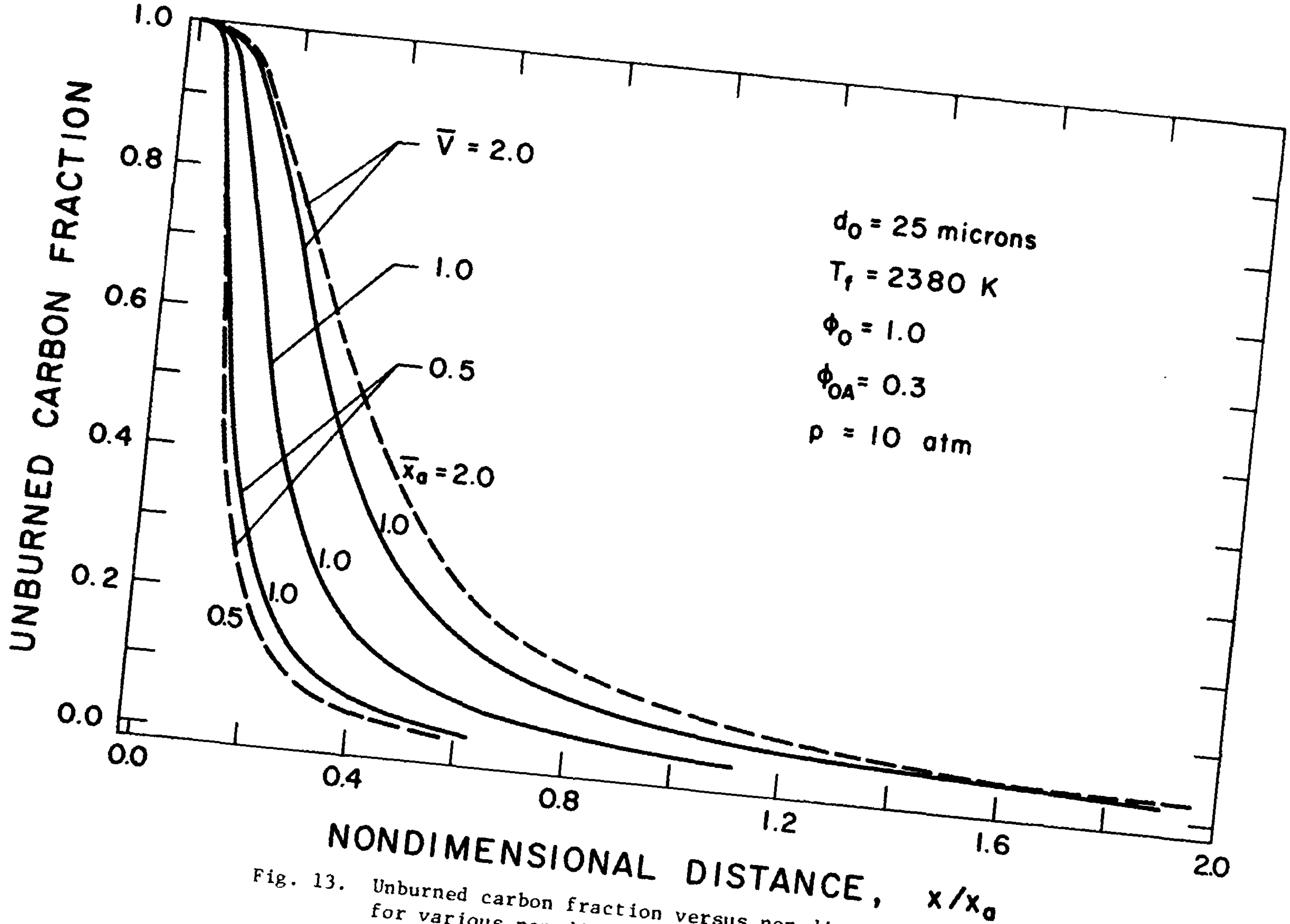

Fig. 13. Unburned carbon fraction versus non-dimensional distance for various non-dimensional reference velocities.

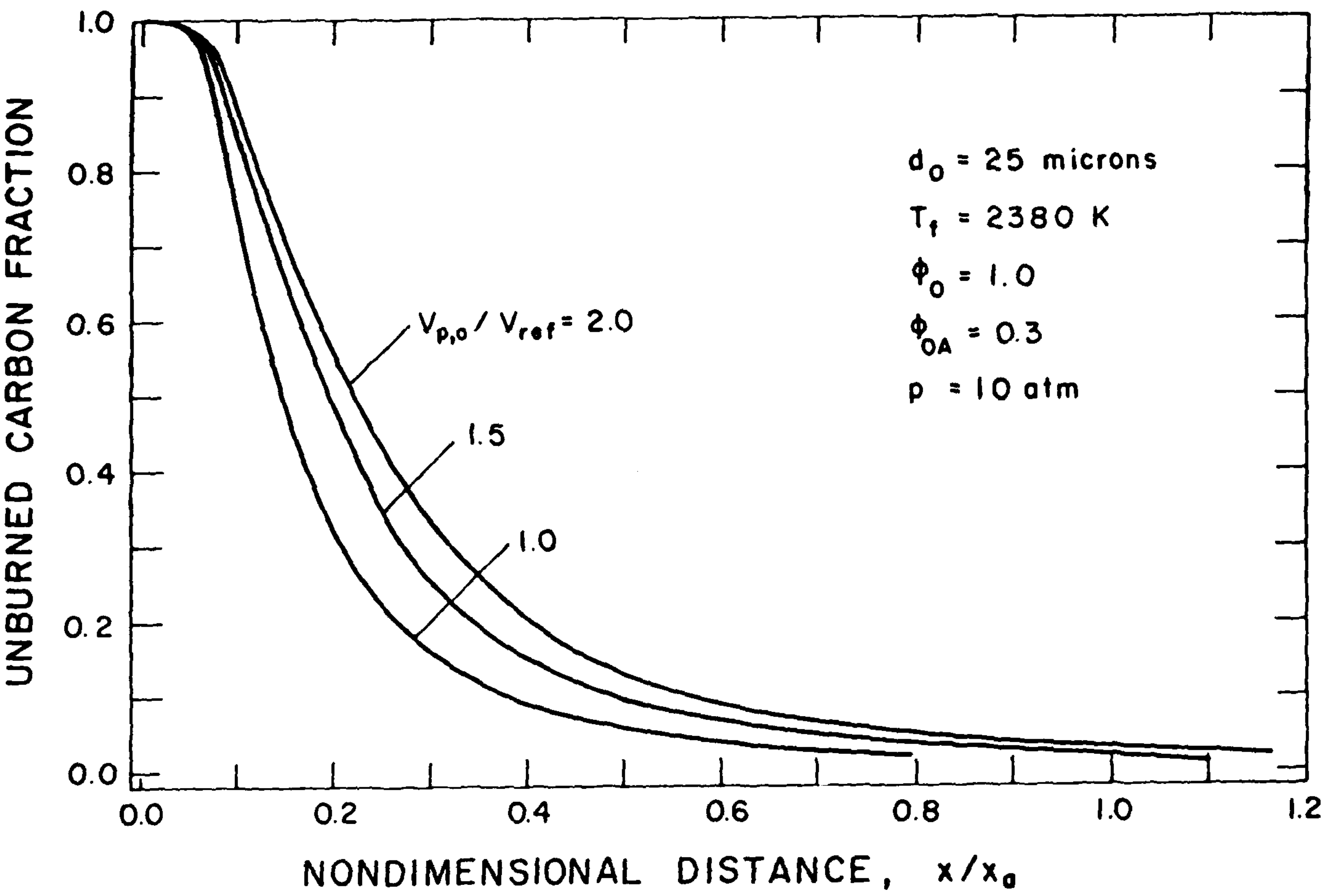

Fig. 14. Unburned carbon fraction versus non-dimensional distance for initial particle slip ratios of 1.0, 1.5 and 2.0.

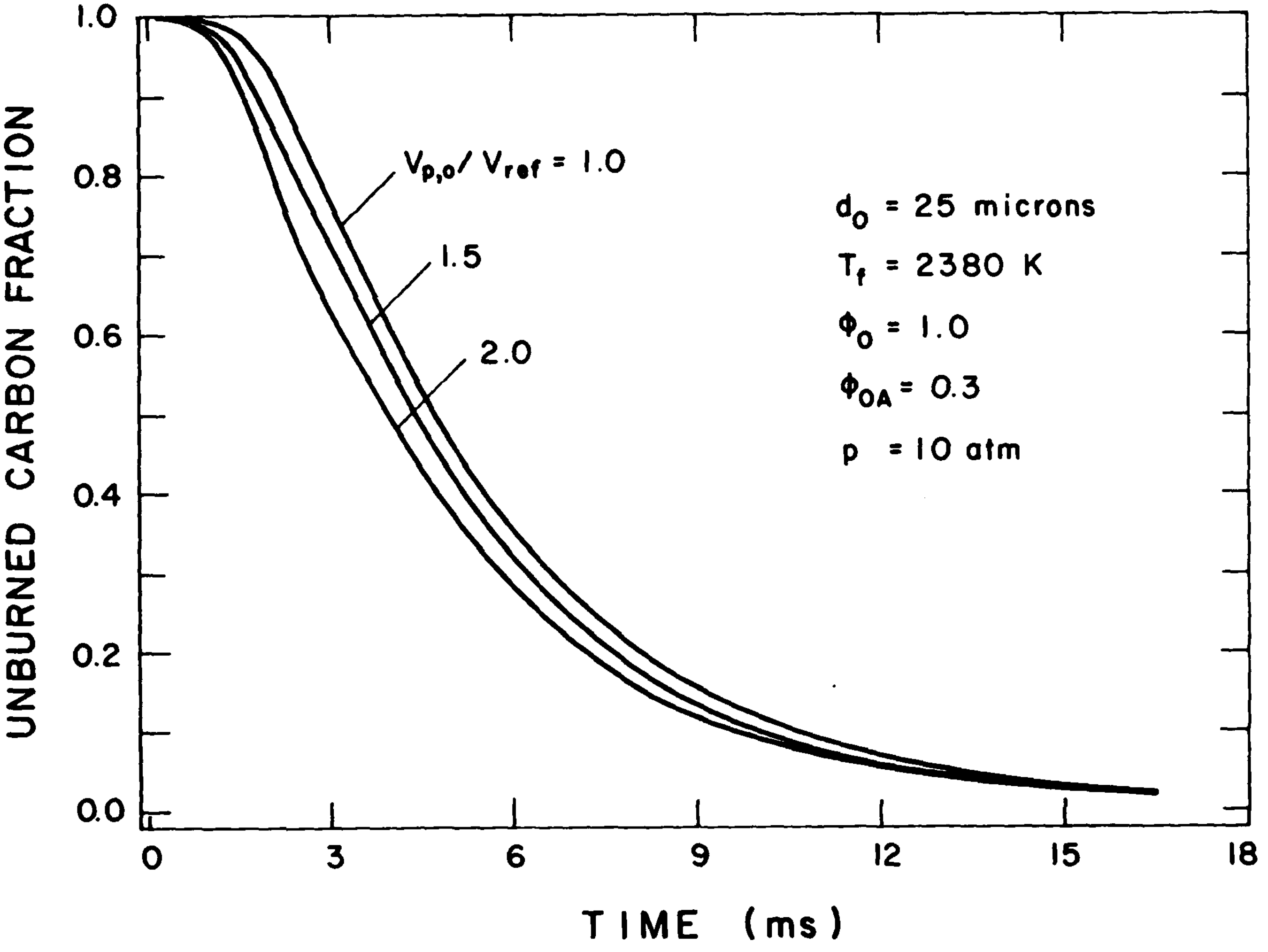

Fig. 15. Unburned carbon fraction versus time for initial particle slip ratios of 1.0, 1.5 and 2.0

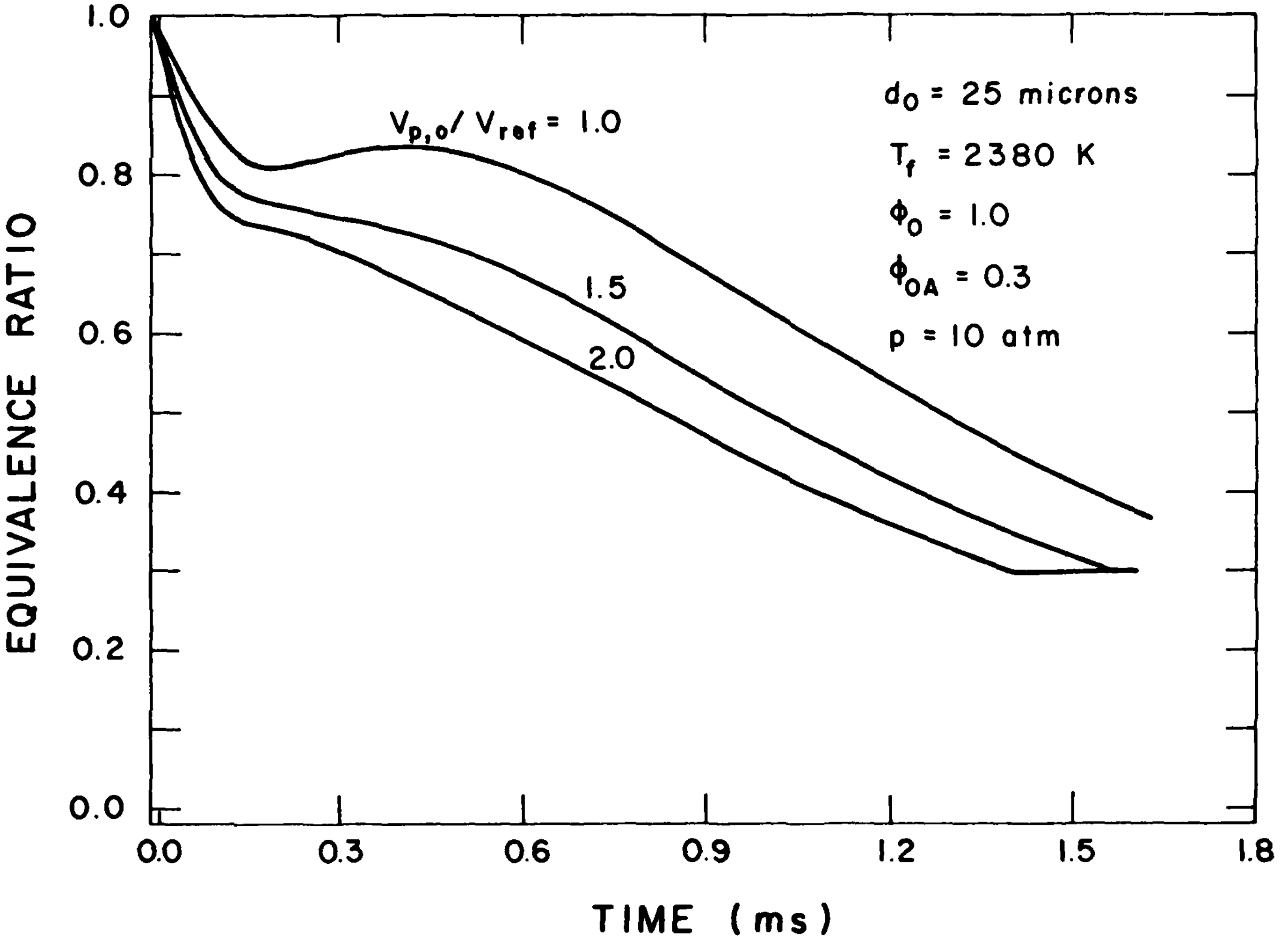

Fig. 16. Gas-phase equivalence ratio versus time for initial particle slip ratios of 1.0, 1.5 and 2.0.

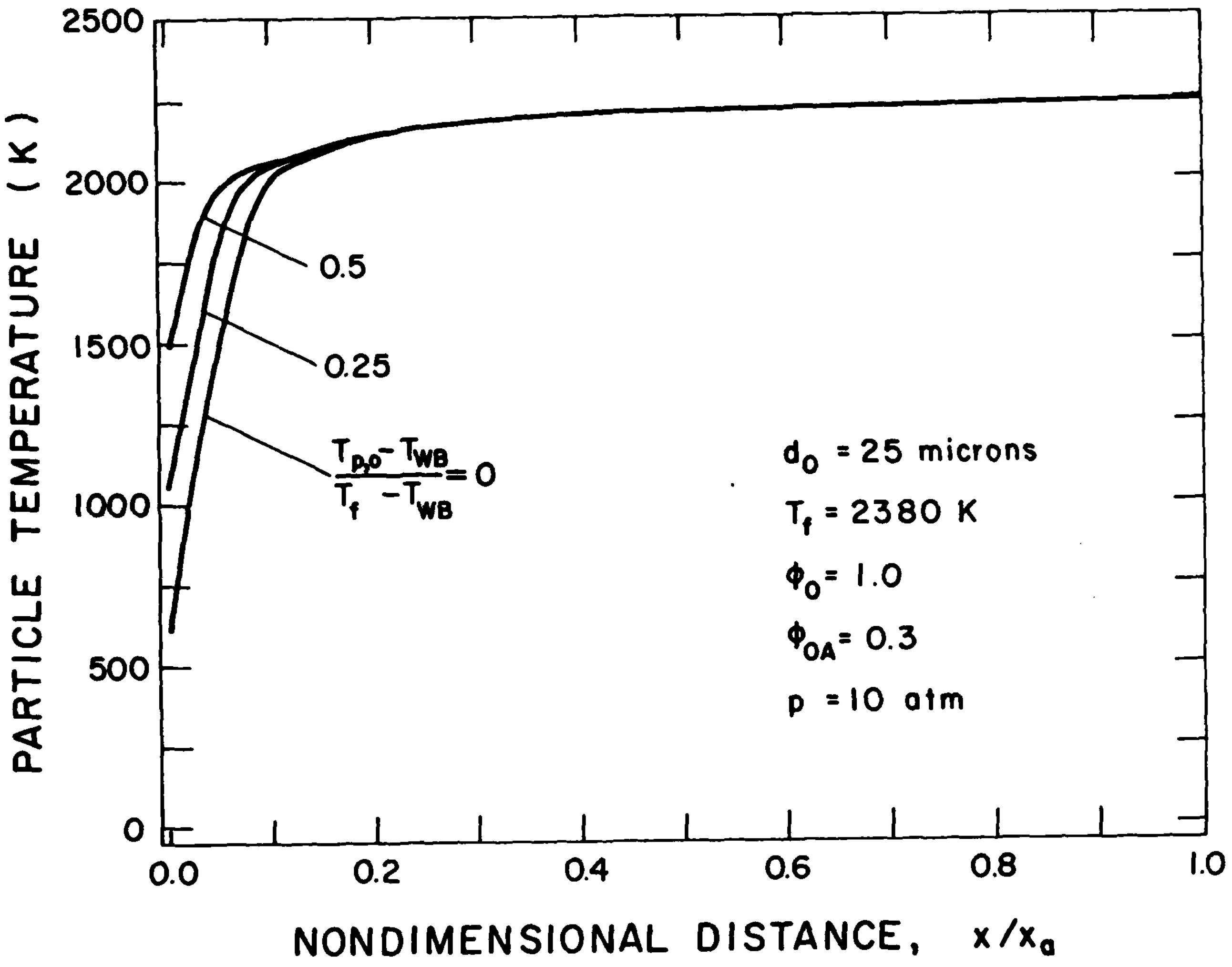

Fig. 17. Particle temperature versus non-dimensional distance for various amounts of agglomerate preheat.

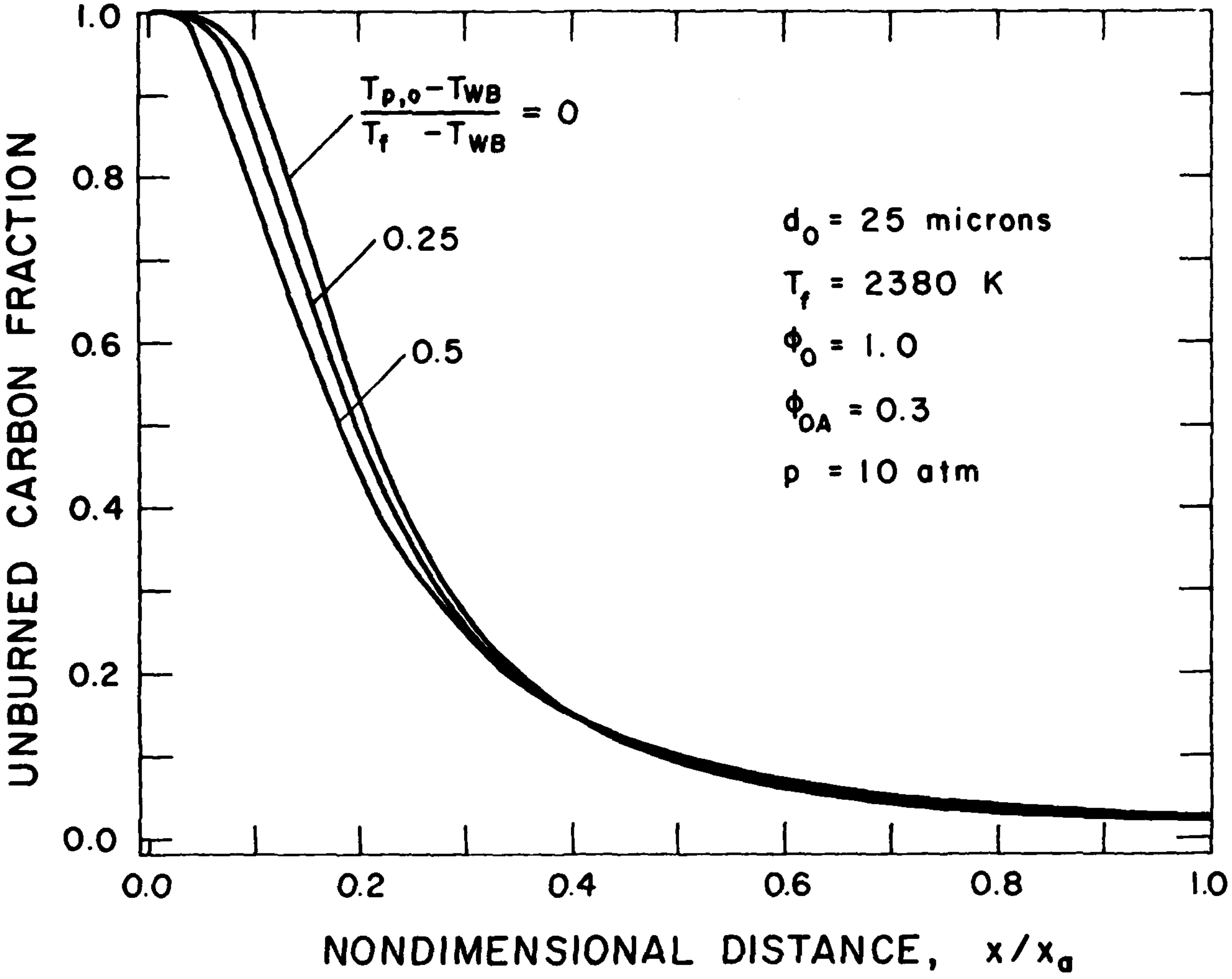

Fig. 18. Unburned carbon fraction versus non-dimensional distance for various amounts of agglomerate preheat.

3.2.8 Agglomerate Composition

The effect of the ultimate size of the carbon-black particles composing the agglomerate particle on carbon burnout also was evaluated for ultimate particle sizes of 300 nm and 70 nm. For all practical purposes, no effect of ultimate particle size was observed. A similar result was obtained when the influence of catalyst addition to the slurry was simulated by applying the appropriate area-reactivity constants given in Szekely and Faeth [9]. These results strongly suggest that the agglomerate microstructure is relatively unimportant in combustion environments of practical importance where diffusion-controlled combustion appears to dominate the carbon burnout process. To provide additional insight into the importance of reaction kinetics, the combustor analysis was repeated at the standard condition for a series of runs in which the area-reactivity factors were varied over a range from 1/20 to twice the values given by Eqs. (4) and (5). The results of this experiment are shown in Fig. 19 where the 97% burnout time is plotted as a function of the ratio of the adjusted area-reactivity factor to the standard value. As the a_i ratio increases, the burnout time approaches an asymptotic value, i.e., the diffusion-limited case. One can observe then that for the standard conditions used in the combustor analysis, the carbon combustion process approaches the diffusion limit--with the near-zero slope indicating only a weak influence of kinetics. This result is consistent with the predicted lack of catalyst influence, as well as the 1.32 power-law exponent obtained for the dependence of burning time on initial particle diameter (Table 3).

3.3 Conclusions

Based on a one-dimensional analysis of carbon slurry-fueled combustor, the following conclusions were obtained:

1. Initial agglomerate diameter, chamber pressure, and secondary air scheduling all had a significant effect on carbon burnout. The effects of diameter and pressure were essentially independent of the extent of reaction or combustion efficiency, while the effect of early air introduction diminished to near zero as combustion efficiencies approached 100%.

2. Increasing combustor reference velocity strongly affected carbon burnout lengths through the combined effects of decreased residence time--causing increased burnout length--and a more oxygen-rich environment for a fixed air injection length--which counteracted the residence time effect to some degree. Burnout times were significantly decreased by the oxygen enrichment effect.

3. The effect of particle preheat was relatively insignificant for combustion efficiencies of practical importance; however, variations in initial particle slip velocity

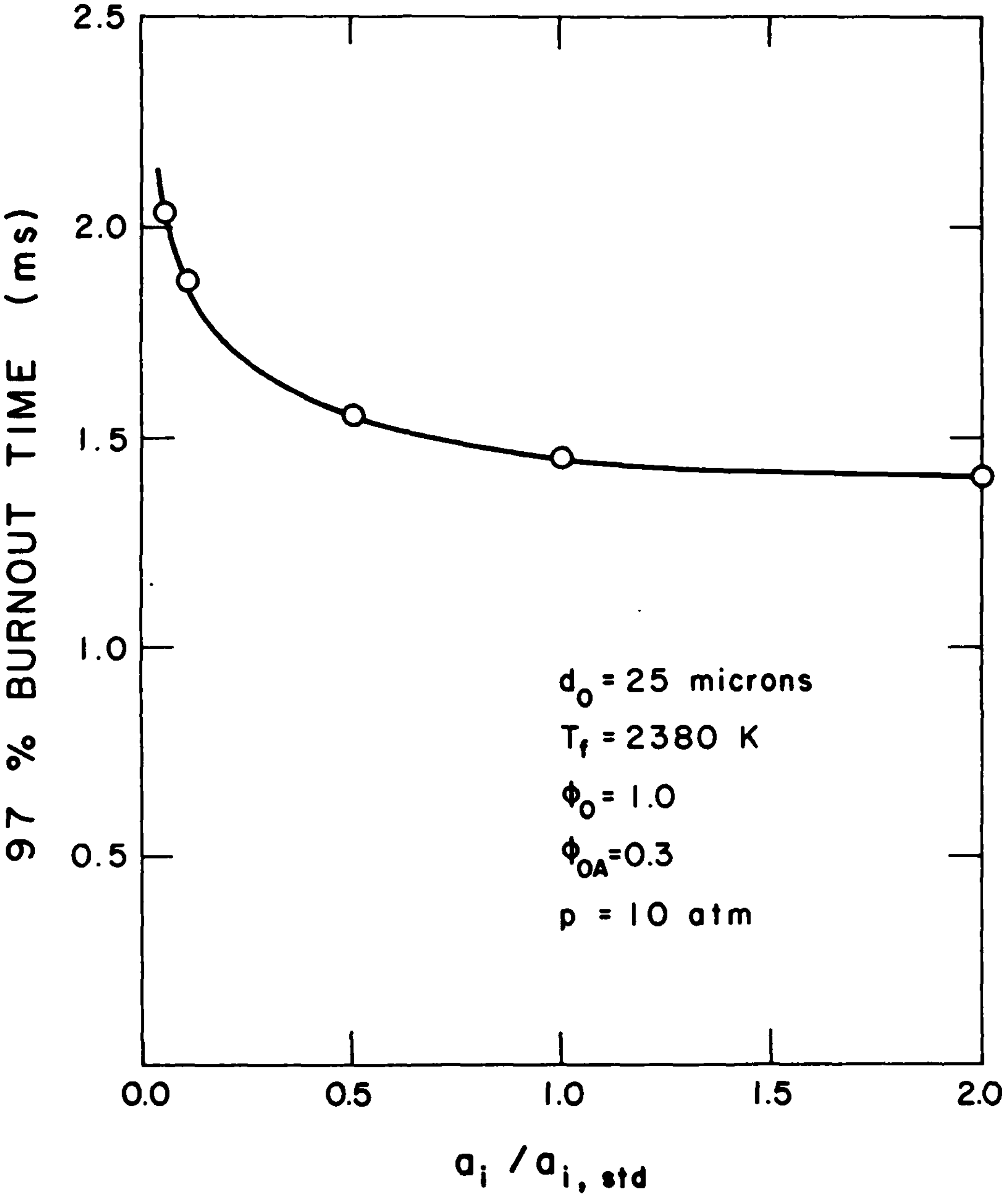

Fig. 19. Effect of area-reactivity factor on the predicted time for 97% carbon burnout.

produced a substantial effect on predicted combustor performance and should be investigated further.

4. The predicted effects of changing ultimate carbon-particle size and addition of catalyst on combustor performance were insignificant--indicating the lack of importance of agglomerate microstructure and reactivity in diffusional-controlled combustion environments typical of practical combustion chamber conditions.

4. Experimental Methods

4.1 Test Apparatus

The test apparatus was based on the supported-particle technique. Slurry drops were evaporated on a slightly enlarged end of a quartz fiber to form agglomerates. The fiber was then mounted so that the agglomerate could suddenly be exposed to a flame environment. Measurements included: temperature and composition of the flame gases, agglomerate diameter as a function of time and agglomerate mass. Provision was also made to quench the process after partial reaction so that surface properties could be observed with a scanning electron microscope (SEM).

A sketch of the apparatus appears in Fig. 20. The arrangement consists of a flat-flame burner, an agglomerate mount and a reaction quenching system. The flat-flame burner was identical to the arrangement used during earlier work in this laboratory [10-12]. The burner was fueled with mixtures of gaseous nitrogen, oxygen, methane and hydrogen. The mixing pressure was monitored with a Heise absolute pressure gauge having a pressure range of 0.0-0.4 MPa. Gas flowrates were controlled with pressure regulators and needle valves and measured with rotameters. All rotameters were calibrated with wet-test meters.

Prior to entering the chamber, gas mixing occurred in a 1.5 m length of 10 mm I.D. tubing. The burner housing was constructed of 51 mm nominal diameter schedule 40 stainless steel welded pipe having a total length of 300 mm. Layers of small beads and voids facilitated mixing and flow uniformity across the burner. The top layer of stainless steel beads stabilized the flame and prevented flashback. A 53 mm I.D., 50 mm long, quartz tube, supported on the burner surface, reduced mixing of the burner and ambient gases until the test position was reached.

The drops were dried on a quartz filament (roughly 200μm diameter) and then baked in an oven at 150°C for one hour to assure complete dryout. The filament was then mounted on a movable support and placed in position at the centerline of the burner with the quenching system in place in order to prevent premature reaction.

The quenching system was a stainless steel tube having a 9 mm I.D. which could be moved over the position of the agglomerate. A flow of nitrogen was maintained through the tube to prevent premature agglomerate reaction and help cool the quenching tube while it was in the hot flame gases. A pneumatic system, controlled with a timer, retracted the quenching tube and terminated the nitrogen flow to rapidly submerge the agglomerate in the flame gases and initiate reaction. This process could be reversed to quench the process at any time. The time required to submerge or quench the reaction was always less than 10 ms.

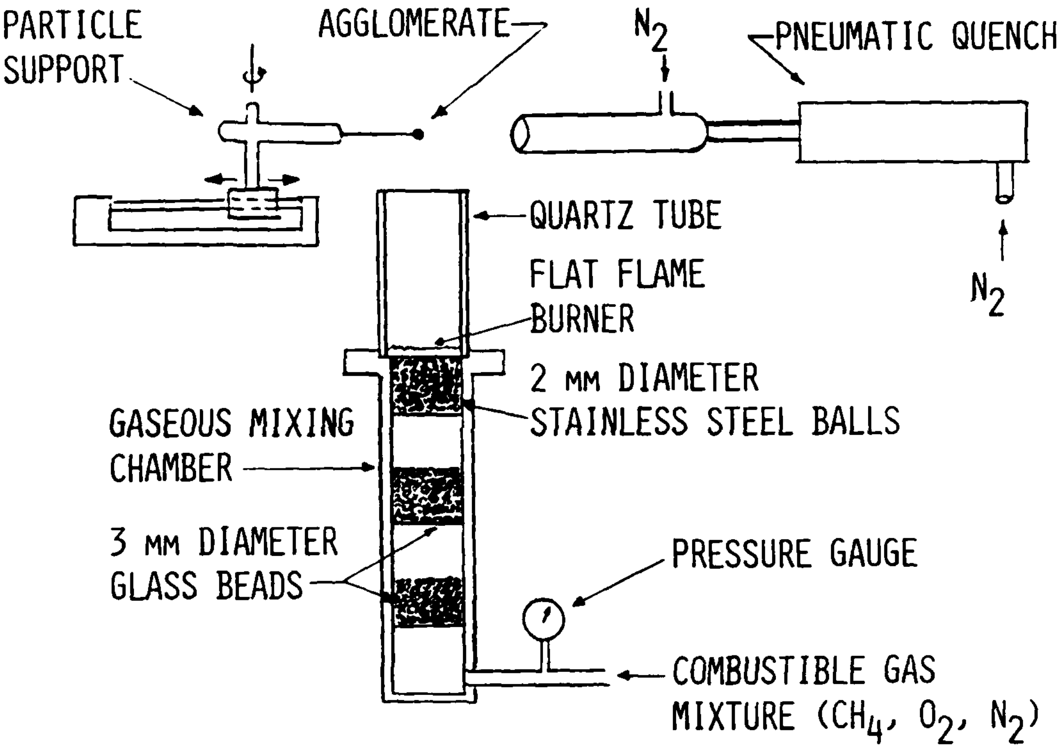

Fig. 20 Sketch of the test apparatus.

4.2 Instrumentation

4.2.1 Agglomerate Environment

Gas temperatures at the location of the agglomerate were measured with a thermocouple probe. The probe was constructed of 25 μm diameter platinum/platinum-10% rhodium wires which were spot-welded to 250 μm diameter lead wires of the same materials, respectively. The emissivity of the thermocouple was taken to be the same as earlier work, 0.22 ± 0.02 [9-12]. The thermocouple was corrected for radiative heat losses following past practice [9-12].

Gas samples were extracted at the agglomerate location using a stainless steel, water-cooled probe having an inlet diameter of 0.7 mm. The temperature of the cooling water was maintained above 340K to avoid condensation of water vapor in the probe. An ice-bath cold trap was placed in the sampling line to condense water prior to analysis. Water vapor concentrations were found using conservation of element analysis.

The samples were analyzed using a gas chromatograph (Varian model 3720) with a thermal conductivity detector. Operating conditions, separating columns and calibration methods are described elsewhere [9-12].

Gas velocities at the measuring location were determined theoretically--assuming one-dimensional flow. These calculations are straightforward, knowing the burner mass flow rate, the gas temperature and composition, and the inside diameter of the quartz shield just below the agglomerate location.

4.2.2 Agglomerate Measurements

The agglomerate combustion process was observed with a 16 mm, Photosonics model 16-B, motion picture camera. The camera optics gave a 2:1 magnification. The camera was powered with a Kepco, SM-36-5 AM d.c. power supply. The film speed was indicated with a neon-timing light within the camera which placed marks on the edge of the film. The timing light was actuated with an Adtrol Electronic pulse generator, model 501. Kodak Plux/X reversal film was used for all tests.

Backlighting of the agglomerate to obtain a shadowgra
presented little difficulty since the test flames were not ous.
This was accomplished with a conventional 60W light bulb pla
roughly 250 mm behind the agglomerate location.

The film records were analyzed on a frame-by-frame basis, using a Vanguard/Bendix motion picture analyzer. The analyzer was equipped with a light pen and digitizing system so that data could be recorded automatically and transmitted to a computer for processing. Photographs of objects of known size at the drop location provided a calibration of distances on the film records. The agglomerate diameters were calculated approximating the agglomerates as ellipsoids (as a spherical diameter for the same volume) [15].

The mass of the particles is too small to be found by conventional weighing. Therefore, a chemical method was used similar to earlier work [9-12]. The quenched agglomerates were placed in a reaction chamber which was evacuated (below 4 kPa) and then heated to 500K for several hours to remove any condensibles. The dried particles were then exposed to an oxygen and hydrogen environment at 85 kPa and 1000K for several hours to react all the carbon. After cooling to room temperature, the concentrations of CO (usually nil) and CO_2 in the chamber were measured using the gas chromatograph. Given the pressure, temperature, volume and carbon fraction of the gas, the mass of the agglomerate can be computed directly. The gas chromatograph system used for these measurements was identical to the system used for the agglomerate environment measurements.

4.3 Test Conditions

Experimental conditions used during the investigation are summarized in Table 4. The temperature, the composition of major gas species, and the velocity were found as described in Section 4.2. Conditions were chosen to provide near diffusion-controlled combustion, near kinetic-controlled combustion and a mixture of these two. Nominal fuel equivalence ratios will be used to describe test conditions in the following--the actual values differ slightly as indicated in Table 4. These test conditions are comparable to those used during earlier work [9-12], but are slightly different due to apparatus modifications which influence flame stability somewhat.

4.4 Slurry Fuel Properties

The slurry fuels were provided by R. S. Stearns and L. W. Hall, Jr. of Sun Tech, Inc., Marcus Hook, PA. The properties of the carbon black dispersed phase are summarized in Table 5. Only carbon black properties are given, since dried agglomerates were tested. The blacks will be designated by their ultimate carbon particle size in the following, e.g., 70, 180 and 350 nm. Most of the tests were conducted with the 70 and 350 nm blacks or blends of these materials.

Table 4. Summary of Flame Properties

ϕ		T	Velocity	Mole Fractions				
Nominal	Actual	(K)	(m/s)	O_2	CO_2	CO	N_2	H_2O
0.6	0.61	1690	1.46	0.088	0.069	--	0.705	0.138
0.6	0.58	1940	2.38	0.107	0.075	--	0.667	0.150
1.0	0.97	1690	0.85	0.006	0.078	0.002	0.754	0.159

Table 5. Carbon Black Properties*

Ultimate Particle Size (nm)	70	180	350
Type	Semi-Reinforcing Furnace	Fine Thermal	Medium Thermal
Designation	SRF	FT	MT
ASTM Code	N770	N880	N990
Surface Area (m^2/g)	25	16	8
Density in Helium (kg/m_3)	1930	1880	1840
Porosity (%)			
Closed	8	11	13
Total	22	21	14
Elemental Concentration (%)			
C	99.2	99.4	99.3
H	0.4	0.5	0.3
O	0.2	0.1	0.1

*Liquid carrier properties are not given since only dried agglomerates were tested.

5. Test Results and Discussion

5.1 Initial Agglomerate Density

Initial diameters for the test agglomerates were in the range 700-800 μm. The densities of these agglomerates, unreacted, was determined during initial tests. Results for pure agglomerates of 70 and 350 nm blacks as well as one blend consisting of 50% (each) by mass of these blacks appear in Table 6. The density values found here are significantly lower than those reported during earlier work [10,11]. This was checked repeatedly during the present study and it is felt that the results appearing in Table 6 are more reliable. The present values are roughly half the density of the blacks in helium, cf., Table 5, which is reasonable in view of the porous nature of the agglomerates.

The measured densities in Table 6 have a relatively high variance. This is largely due to the irregular geometry of dried agglomerates. There is no statistically significant difference between the densities of agglomerates of the pure carbon blacks in Table 6. However, the blend has a higher density, which is expected due to the capability of the small particles to fill up void spaces between the large particles.

5.2 Surface Structure

The appearance of unburned agglomerates was similar to results found during earlier work with both supported and freely-moving agglomerates [9-14]. The particle surface was relatively smooth with the agglomerate more-or-less spherical.

The development of surface structure as reaction proceeds was investigated by quenching agglomerates and then observing the surface with a SEM. Some typical results are illustrated in Figs. 21-26. In each case, photographs are shown at two magnifications: roughly 700X and 2500X. Two flame conditions are illustrated: $\phi = 0.6$, $T = 1940K$ and $\phi = 1.0$ and $T = 1690K$. The time of agglomerate combustion is much different for these two conditions: particles having initial diameters of 700-800 μm burn in 5-10s for $\phi = 0.6$ and $T = 1940K$ while they burn in 10-20 min for $\phi = 1.0$ and $T = 1690K$. For each flame condition, results are shown for neat blacks having ultimate carbon particle sizes of 70 and 350 nm, as well as a blend consisting of equal masses of these sizes. Two sets of photographs are presented for each condition: one set taken at 20-30% of the combustion lifetime, and one set at roughly two-thirds of the combustion lifetime.

In general, the surface structure is porous and the degree of porosity increases as reaction proceeds. The sizes of the largest pores are roughly correlated with the ultimate particle size of the carbon black: smallest for the SRF black ($d_u = 70$ nm), largest for the MT black ($d_u = 350$ nm) and intermediate for the blends of these two blacks.

Table 6. Summary of Initial Agglomerate Densities

Slurry Composition	Density (kg/m^3) Mean Value	Density (kg/m^3) Variance
Pure 70 nm black	1090	70
Pure 350 nm black	1110	80
50% (ea) by mass, 70 and 350 nm blacks	1230	110

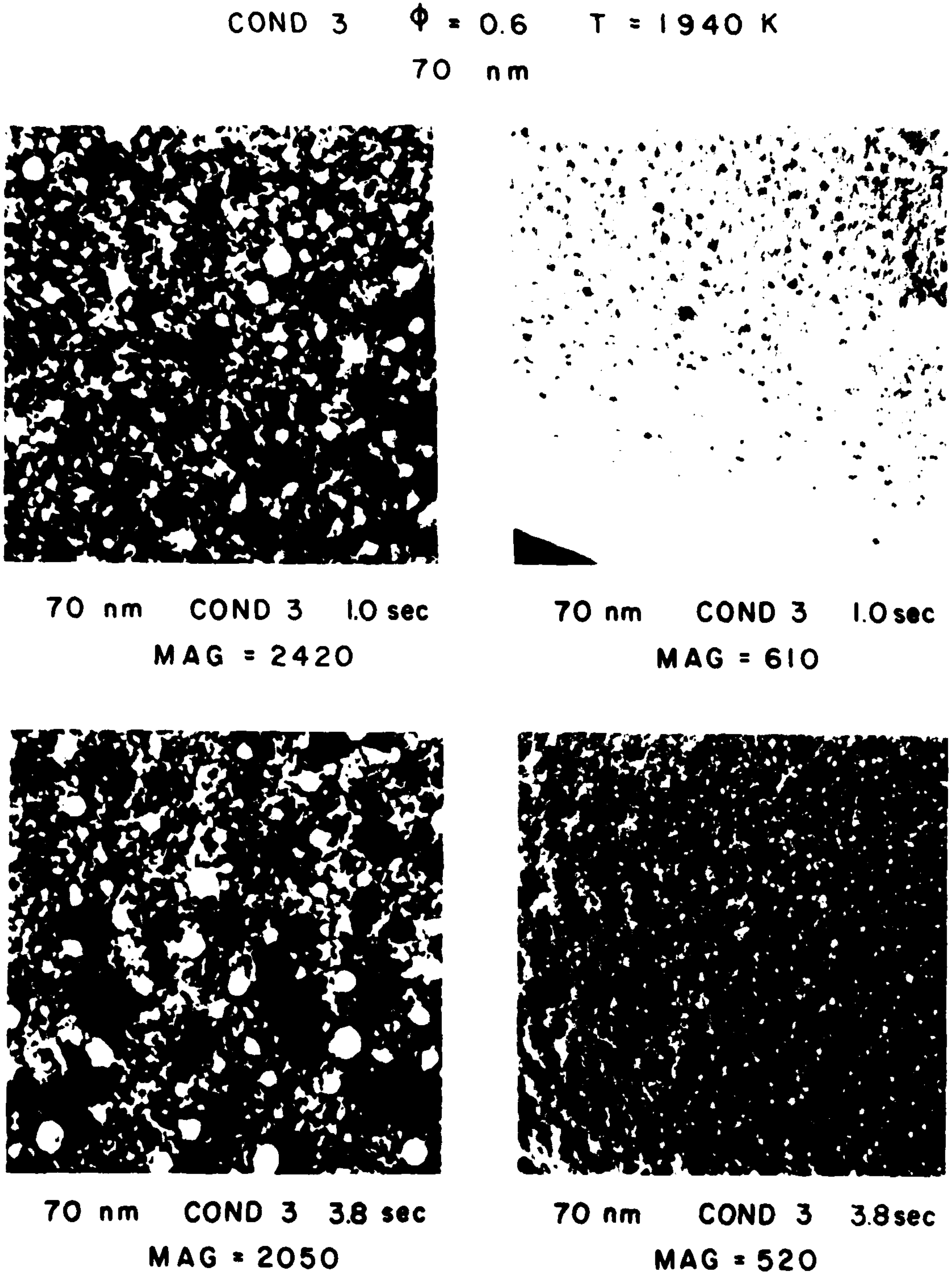

COND 3 Φ = 0.6 T = 1940 K
70 nm

70 nm COND 3 1.0 sec
MAG = 2420

70 nm COND 3 1.0 sec
MAG = 610

70 nm COND 3 3.8 sec
MAG = 2050

70 nm COND 3 3.8 sec
MAG = 520

Fig. 21. Surface structure for d_u = 70 nm, ϕ = 0.6, T = 1940K.

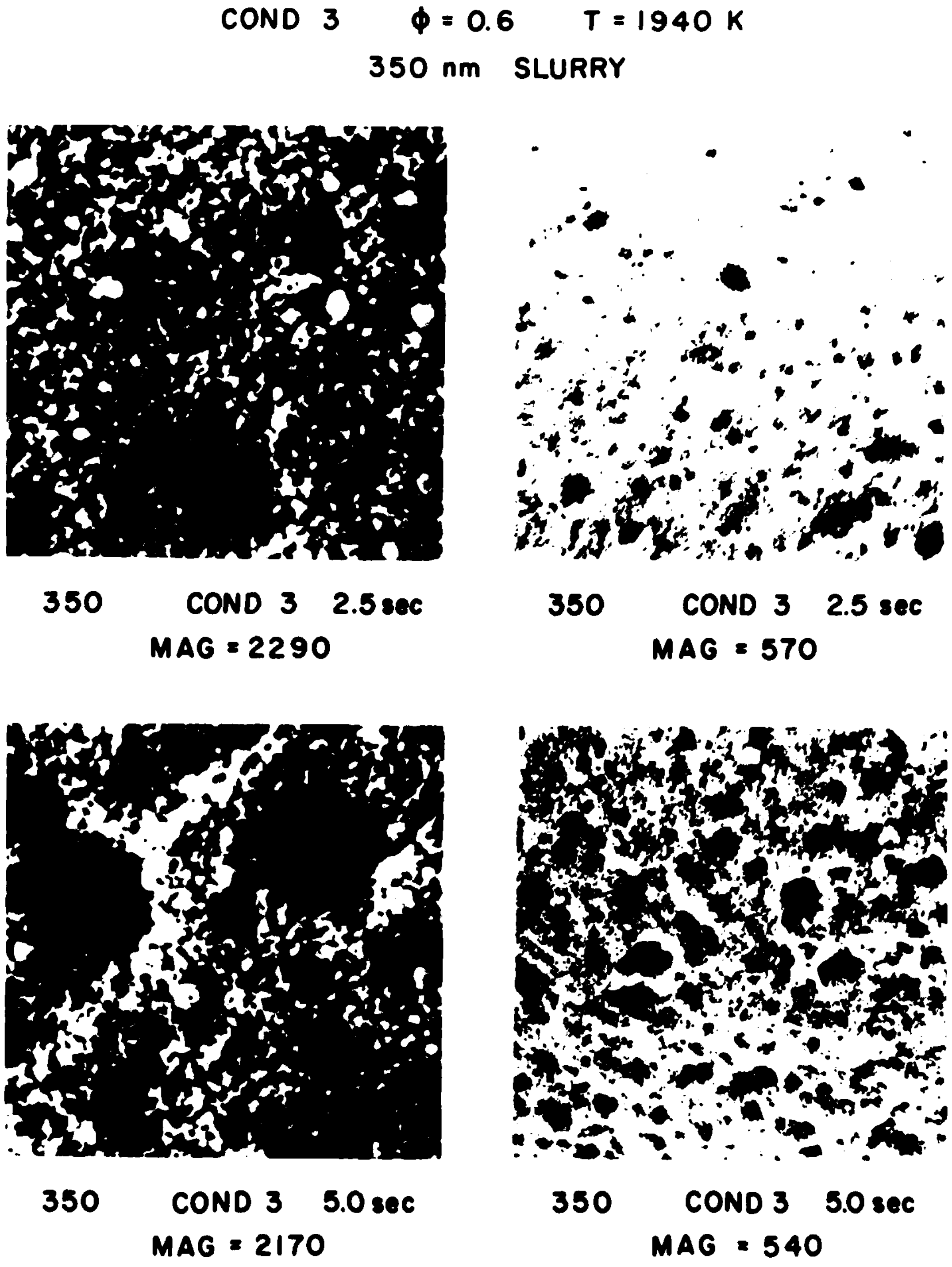

Fig. 22. Surface structure for d_u = 350 nm, ϕ = 0.6, T = 1940K.

COND 3 $\Phi = 0.6$ $T = 1940$ K
50 % 350/50 % 70 BY MASS

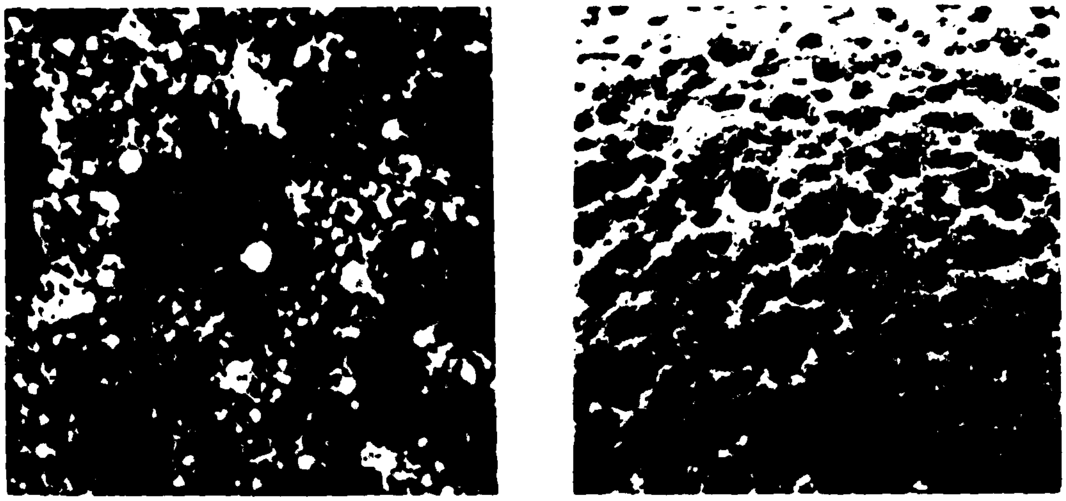

50 / 50 COND 3 2.4 sec
MAG = 2350

50 / 50 COND 3 2.4 sec
MAG = 610

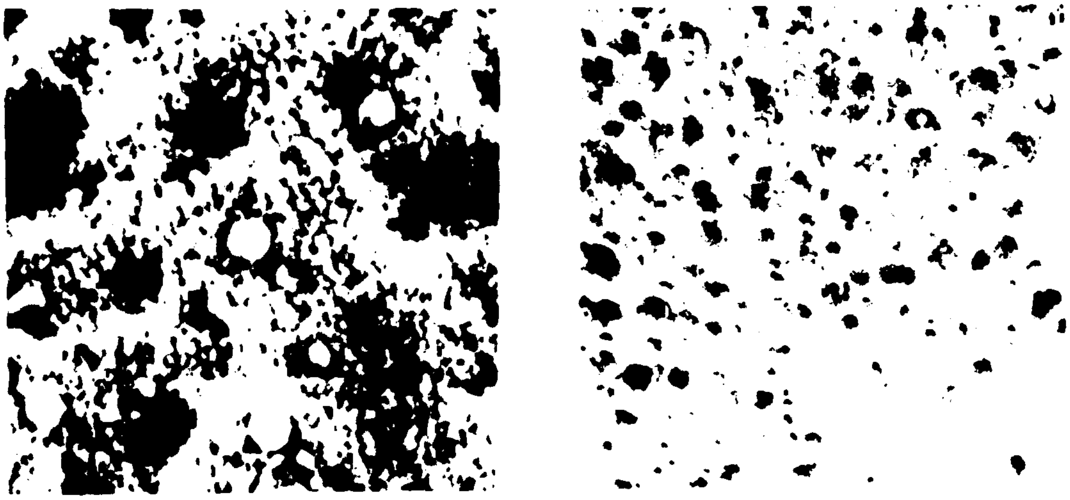

50 / 50 COND 3 4.8 sec
MAG = 2020

50 / 50 COND 3 4.8 sec
MAG = 530

Fig. 23. Surface structure for bimodal blend with $d_u = 70$ and 350 nm (50% each by mass), $\phi = 0.6$, $T \cong 1940$K.

COND 2 $\Phi = 1.0$ T = 1690 K

70 nm SLURRY

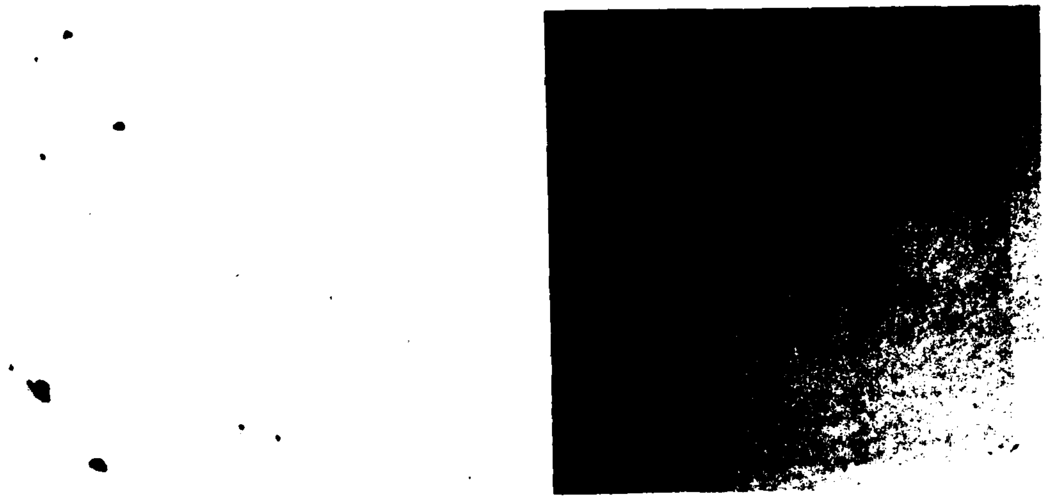

70 nm COND 2 3 min
MAG = 2470

70 nm COND 2 3 min
MAG = 740

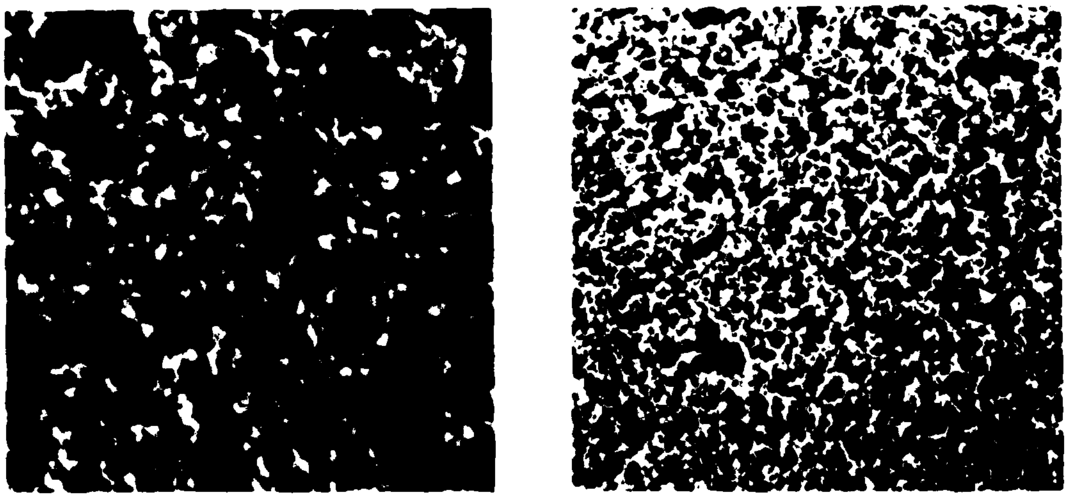

70 nm COND 2 6 min
MAG = 2460

70 nm COND 2 6 min
MAG = 630

Fig. 24. Surface structure for d_u = 70 nm, ϕ = 1.0, T = 1690K.

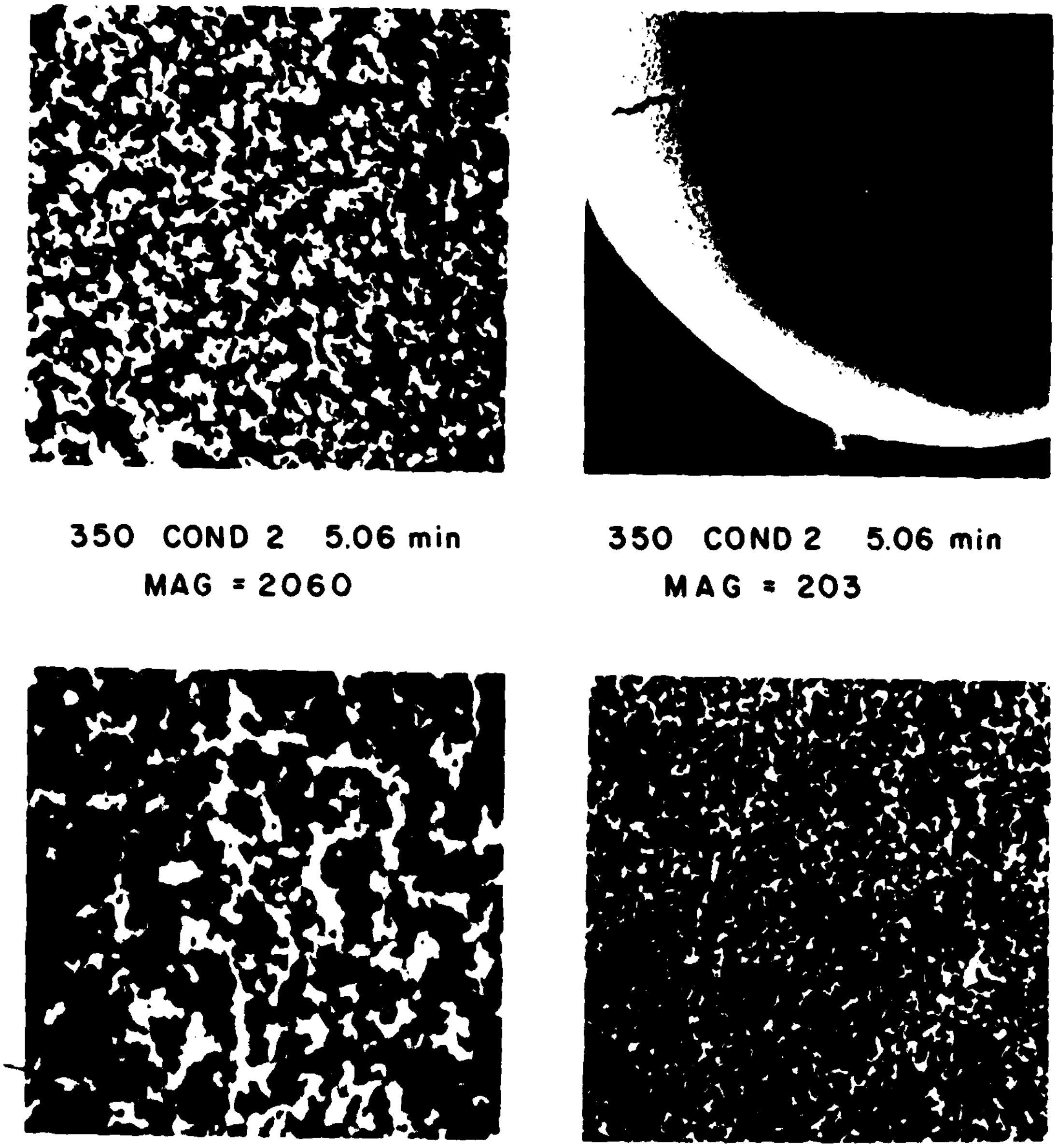

COND 2 Φ = 1.0 T = 1690 K

350 nm SLURRY

350 COND 2 5.06 min
MAG = 2060

350 COND 2 5.06 min
MAG = 203

350 COND 2 10.1 min
MAG = 2480

350 COND 2 10.1 min
MAG = 680

Fig. 25. Surface structure for d_u = 350 nm, ϕ = 1.0, T = 1690K.

50/50 COND 2 4.67 min
MAG = 2120

50/50 COND 2 4.67 min
MAG = 760

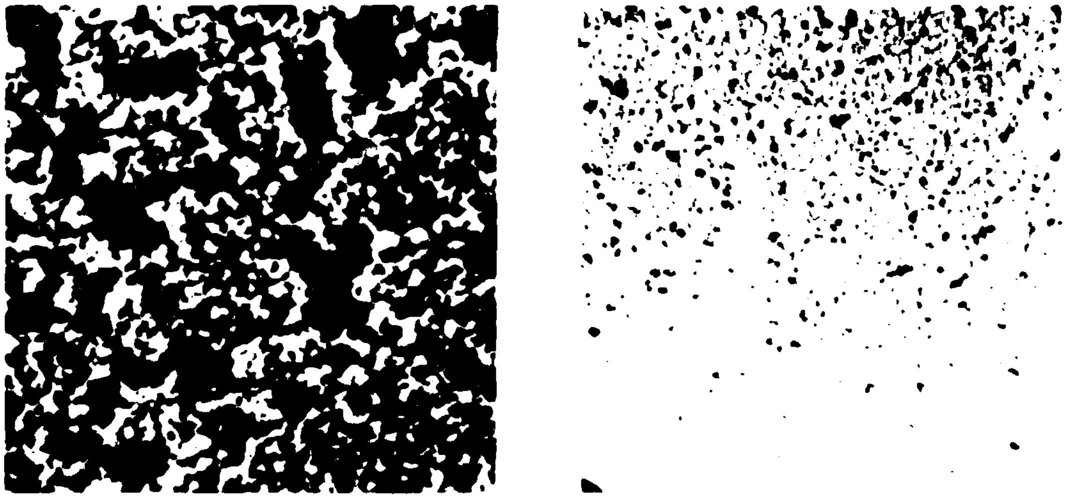

50/50 COND 2 9.33 min
MAG = 2470

50/50 COND 2 9.33 min
MAG = 640

Fig. 26. Surface structure for bimodal blend with d = 70 and 350 nm (50% each by mass), $\phi = 1.0$, $T \cong 1690$K.

The general appearance of the pore structure is similar for the two flame conditions, even though the time of combustion is more than an order of magnitude longer for the higher equivalence ratio. A major difference between the two flame conditions is the appearance of round structures at the lower fuel equivalence ratio condition where particle temperatures are highest. It is likely that these structures are due to melting of impurities in the black (ash) with subsequent coagulation into spheres. Similar behavior has been observed in this laboratory for tests with coal slurries which generally have much higher levels of ash than carbon blacks. Naturally, coalescence of impurities of this type would be less significant for smaller agglomerates more typical of practical combustion chamber conditions, since less impurity would be present in each agglomerate and times available for coalescence are much shorter.

Difficulty was encountered with impurities for the SRF black having an ultimate carbon particle size of 180 nm. In this case, impurities formed a porous shell-like structure having nearly the same size as the original agglomerate even though carbon combustion rates were fast. Since this black had not received much attention during fuel development efforts, tests with this material were not pursued any further.

5.3 Burning Rates

5.3.1 Blends

All data obtained during the investigation are summarized in the appendix. Typical agglomerate life histories (the variation of particle diameter with residence time in the burner gases) are illustrated in Figs. 27-29--each figure representing one of the flame conditions considered during the tests. Three agglomerate compositions are shown on each figure: a neat sample with d_u = 70 nm, a neat sample with du = 350 nm and a blend containing 50% by mass of each of these materials. Initial agglomerate diameters are in the range 740-760 μm for the results pictured in Figs. 27-29.

The results illustrated in Figs. 27-29 are qualitatively the same. The diameter changes relatively slowly just after the agglomerate is submerged in the flame. In this period, the agglomerate heats up from room temperature and reaction rates are low due to the low temperature of the carbon. As the heat-up period ends, the rate of reduction of the diameter begins to increase and generally continues to increase throughout the subsequent lifetime of the agglomerate.

The time of combustion varies with both carbon-black composition and flame condition for the results pictured in Figs. 27-29. In general, the time of combustion is shortest for d_u = 70 nm, longest for d_u = 350 nm and intermediate for the blend of these materials. The time of combustion is strongly influenced by flame condition,

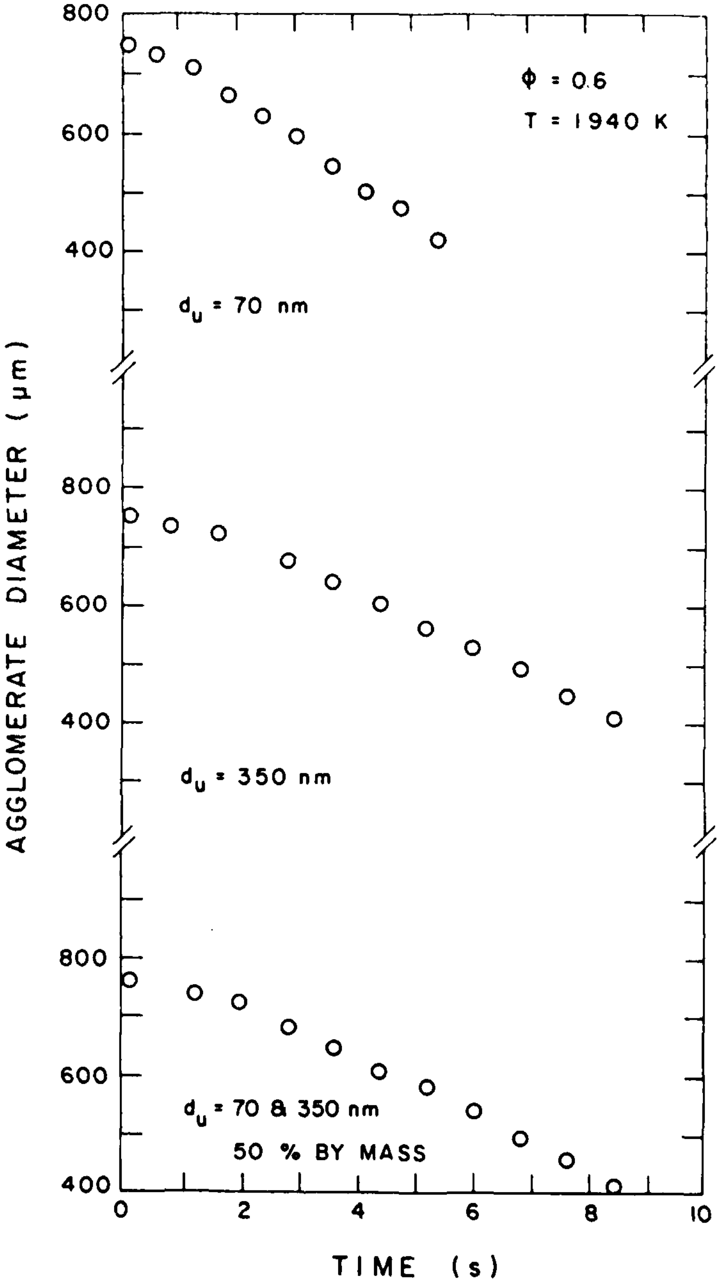

Fig. 27. Agglomerate diameter versus time for $\phi = 0.6$, $T = 1940K$.

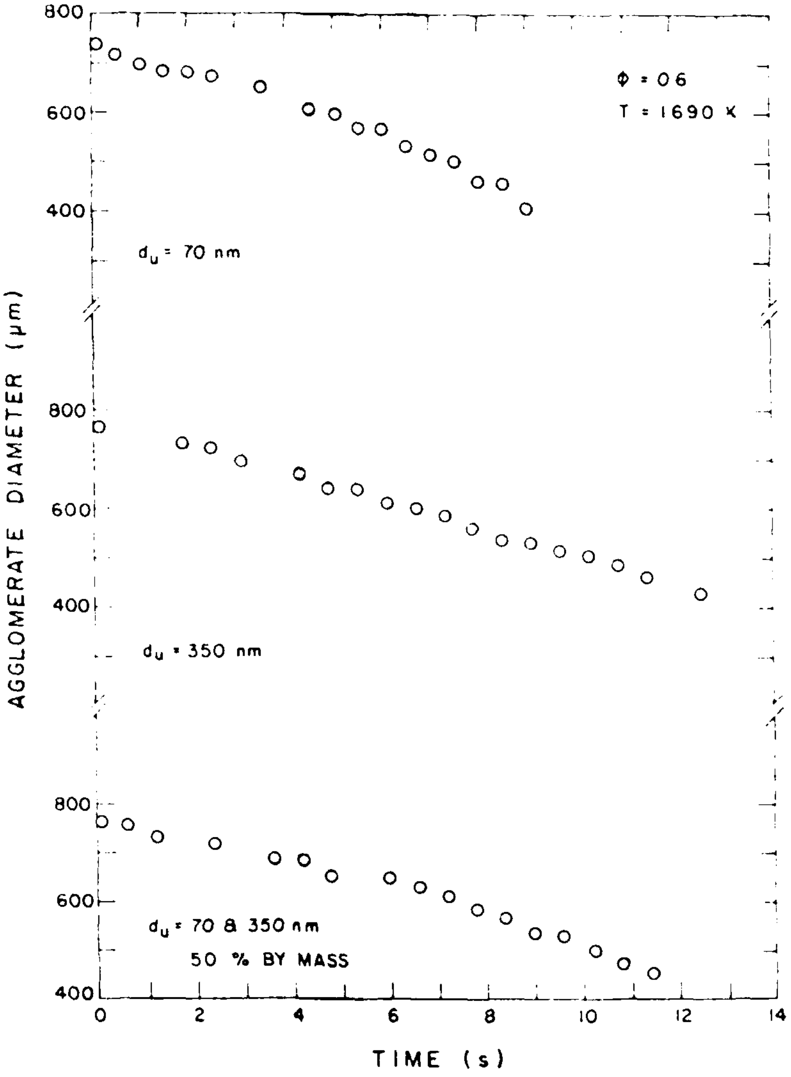

Fig. 28. Agglomerate diameter versus time for Φ = 0.6, T = 1690K.

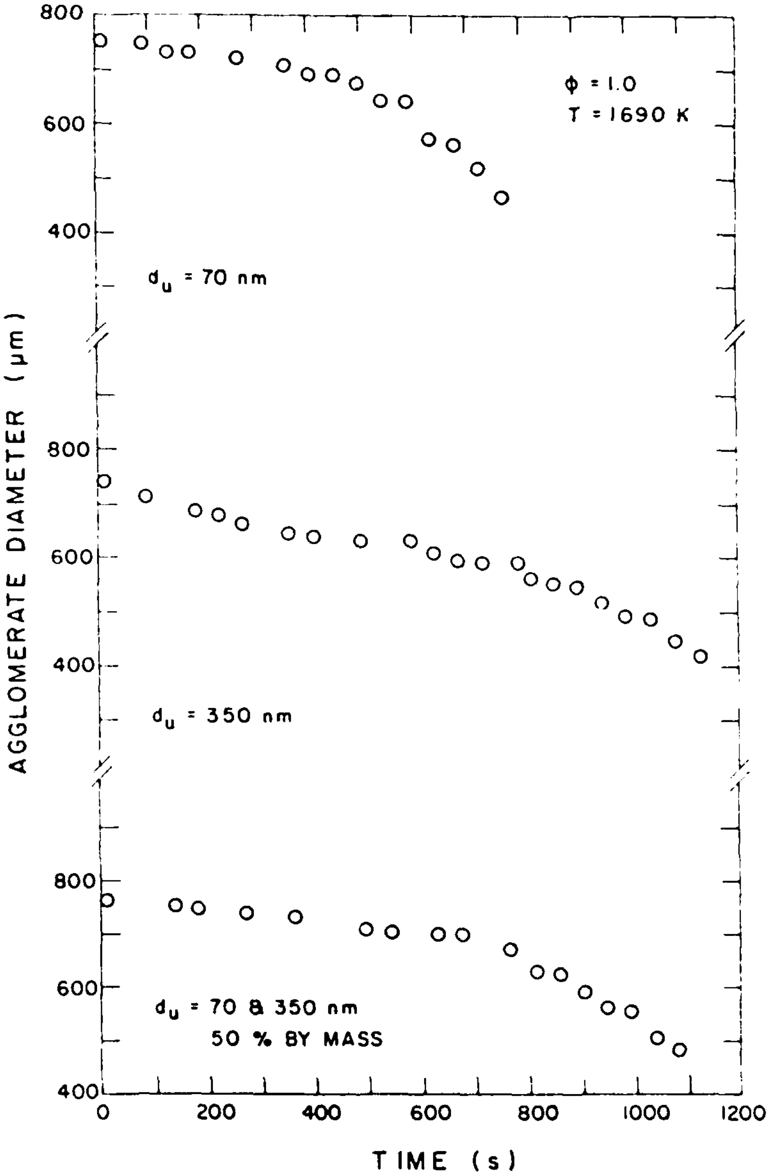

Fig. 29. Agglomerate diameter versus time for ϕ = 1.0, T = 1690K.

being 6-8s for $\phi = 0.6$ and $T = 1940K$, 10-12s for $\phi = 0.6$ and $T = 1690K$ and 1000-1200s (roughly two orders of magnitude longer!) for $\phi = 1.0$ and $T = 1690K$. For the low equivalence ratio conditions, carbon reaction is dominated by reaction with oxygen [9-14]. For $\phi = 1.0$, oxygen concentrations are low and results of Neoh et al. [17] suggest that reaction proceeds via OH; therefore, reaction rates are relatively low due to the low levels of OH found at equilibrium at this condition.

In order to conveniently compare results at different conditions, the volumetric burning rate (burning rate) was defined, similar to past work [9-14]

$$K_v = - \frac{d\,d_p}{dt} \qquad (21)$$

This parameter was only found for $d_p \leq 700\ \mu m$, where the initial particle diameter was roughly 750 μm, in order to eliminate effects of the heat-up period where the agglomerate has not yet reached temperatures representative of steady burning at the local ambient environment [9-14]. The volumetric burning rates were measured for several agglomerate lifetimes in most cases, obtaining both a mean value and a standard deviation. The number of conditions used in each case can be inferred from the data summary appearing in the Appendix.

Burning rates for the same conditions as Figs. 27-29 are plotted as a function of agglomerate diameter in Figs. 30-32. The symbols on the figures indicate the mean value while the bars extend ± one standard deviation. In general, burning rates are largest for the pure carbon black with $d_u = 70$ nm, slowest for $d_u = 350$ nm and intermediate for the blend. These changes are in the range 10-40% for the conditions shown.

The burning rates illustrated in Figs. 30-32 generally increase as d_p decreases--often approaching a constant value at small d_p. Increasing burning rate with decreasing d_p is indicative of diffusion-control of the rate of combustion, where the rate of carbon reaction is limited by the capability of the flow field around the agglomerate to transport oxidant to the surface [9-14]. Relatively constant values of the burning rate with variations of d_p are indicative of kinetic-control, where the rate of carbon reaction is limited by chemical reaction rates at the agglomerate surface and the transport capability of the flow field is only partly utilized. Conditions in Figs. 30-32 exhibit both types of behavior--tending toward kinetic-control as d_p decreases.

The present assessment of diffusion- and kinetic-controlled conditions should be qualified, however, due to effects of the development of the pore structure of the particles, which tends to increase both transport rates (due to flow through the porous particle as represented by increased values of the transport enhancement factor) and surface reaction rates (due to increased

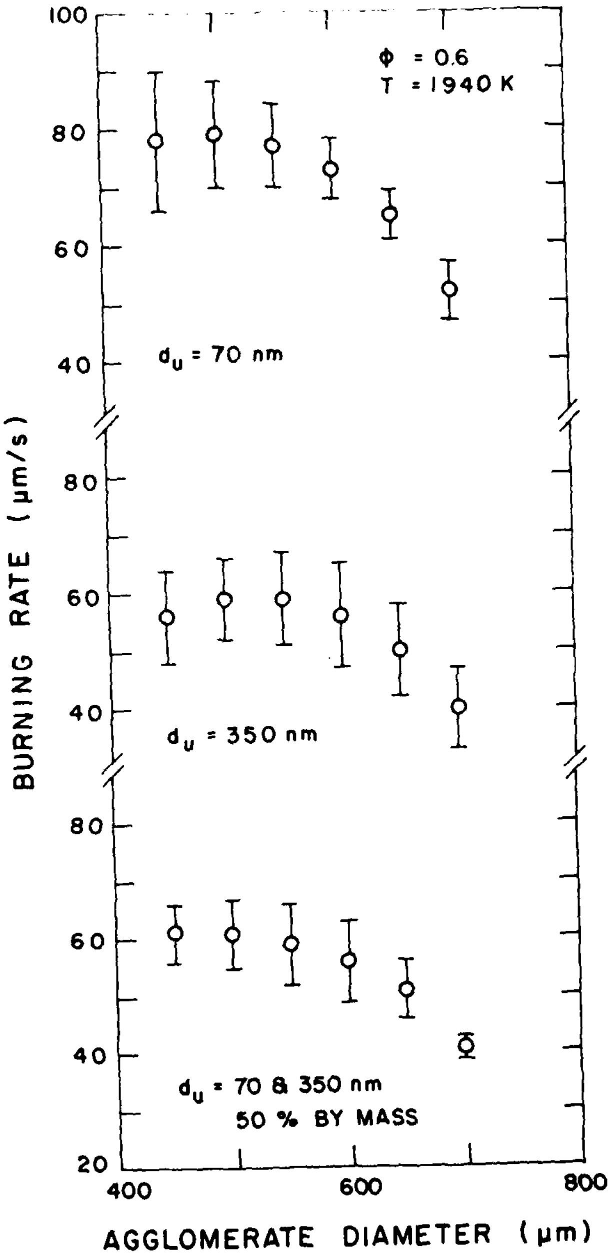

Fig. 30. Agglomerate burning rate versus diameter for ϕ = 0.6, T = 1940K.

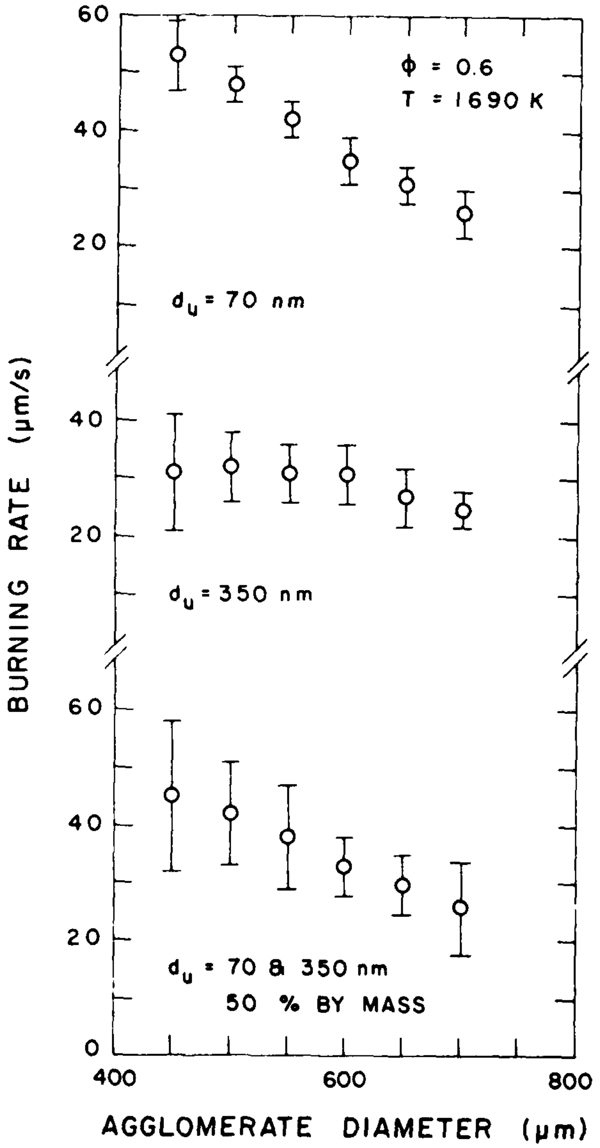

Fig. 31. Agglomerate burning rate versus diameter for $\phi = 0.6$, T = 1690K.

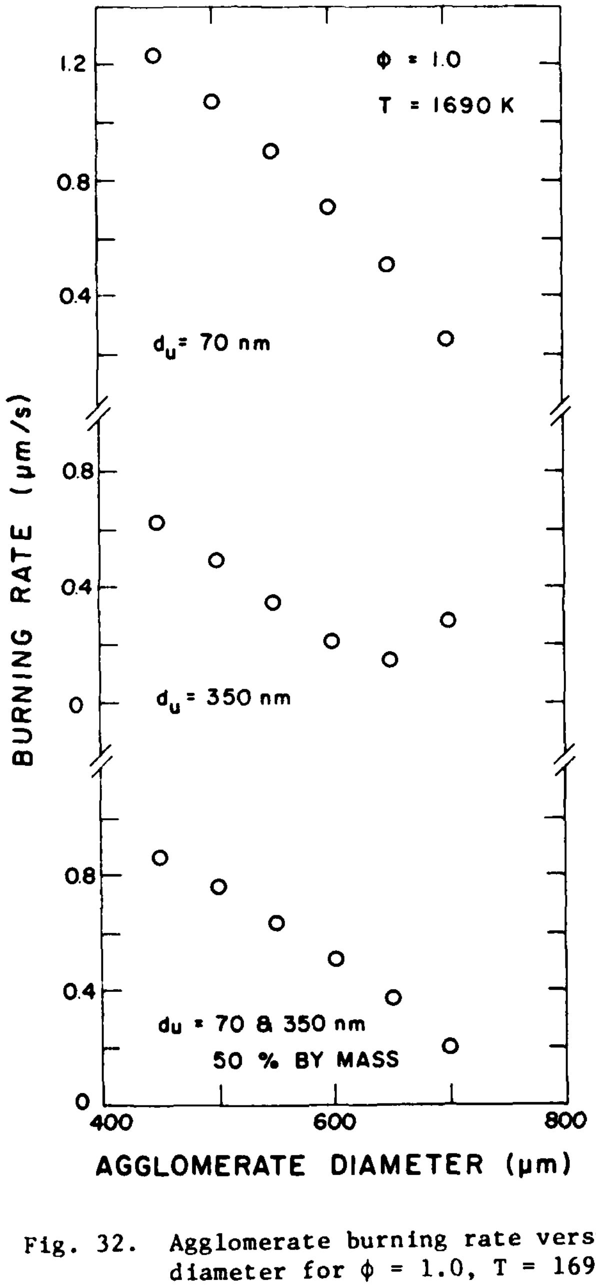

Fig. 32. Agglomerate burning rate versus diameter for ϕ = 1.0, T = 1690K.

surface area as represented by the empirical area-reactivity factors). The transport enhancement factor increases to the greatest degree, particularly when the extent of reaction is less than 50%. This would involve agglomerate diameters in the range 600-750 μm for present test conditions--corresponding to the range where greatest changes in burning rates are observed in Figs. 30-32. Therefore, fully resolving the degree of kinetic- and diffusion-control for these tests will involve application of the agglomerate combustion model--similar to past work [9-14].

The effect of carbon-black composition on burning rates can be seen more directly on the plots illustrated in Figs. 33-35. In this case, burning rate is plotted as a function of % weight of the carbon black with d_u = 350 nm for bimodal carbon-black mixtures containing blacks with d_u = 70 and 350 nm. Initial agglomerate diameters were roughly 750 μm--results are shown for d_p = 450, 550 and 650 μm. In general, results at d_p = 450 μm approach kinetic-control while results at d_p = 650 μm are more representative of diffusion-control--subject to uncertainties concerning effects of pore structure development noted earlier.

The results illustrated in Figs. 33-35 indicate a monotonic decrease in burning rate as the concentration of the carbon black having larger ultimate carbon particle size is increased. The effect of carbon-black composition is generally greatest for conditions where the process is kinetic-controlled, e.g., ϕ = 0.6 and T = 1940K (cf., Fig. 30). Results for ϕ = 1.0 and T = 1690K exhibit similar trends as the other conditions, but there is a large degree of scatter. This is due to variations in ambient oxygen concentration near ϕ = 1, which are very difficult to control during the experiments. In general, there is little tendency for burning rates to approach a minimum at some intermediate blend, as suggested by limited data obtained during earlier work [13,14].

5.3.2 Catalyst

Early work on carbon-black slurry combustion demonstrated that addition of lead catalyst to the slurry increased burning rates at low equivalence ratios [9-12]. Therefore, tests were undertaken to study effects of lead catalyst for carbon-black having d_u = 350 nm. The tests were conducted at ϕ = 0.6 and T = 1690K. Similar to past work [9-12], the catalyst was added to the liquid carrier as a lead salt of an organic acid. In the following, the concentration of catalyst is quoted as the concentration originally placed in the carrier--assuming that all the non-volatile lead salt remained on the agglomerate after drying was complete.

Results of the catalyst tests are illustrated in Fig. 36. The burning rate is plotted as a function of lead concentration (g Pb/kg C) for d_p = 450, 550 and 650 μm. Increasing the lead content results in a substantial increase in the burning rate, by as much as a factor of two, particularly for the range 0-0.25 g Pb/kg C. Greatest changes are observed at kinetic-controlled conditions, e.g., d_p = 450 μm. At higher lead concentrations, the burning rate becomes

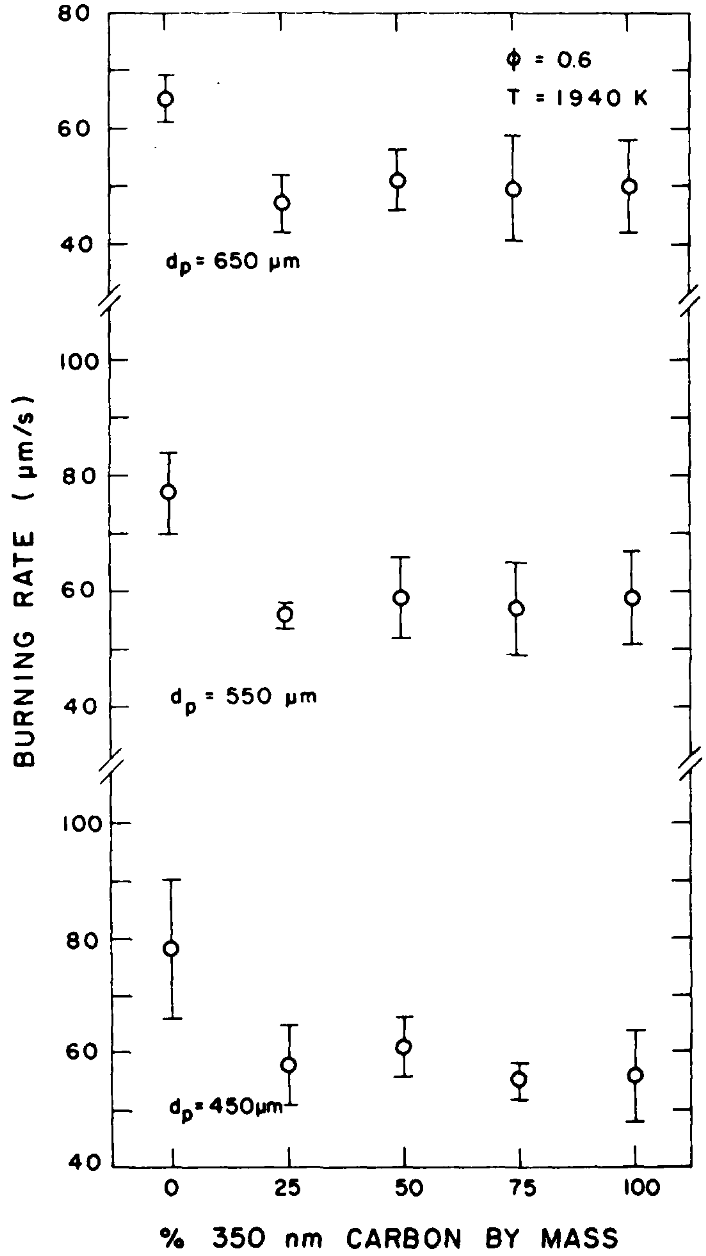

Fig. 33. Agglomerate burning rate versus carbon-black composition (d_u = 70 and 350 nm) for ϕ = 0.6, T = 1940K.

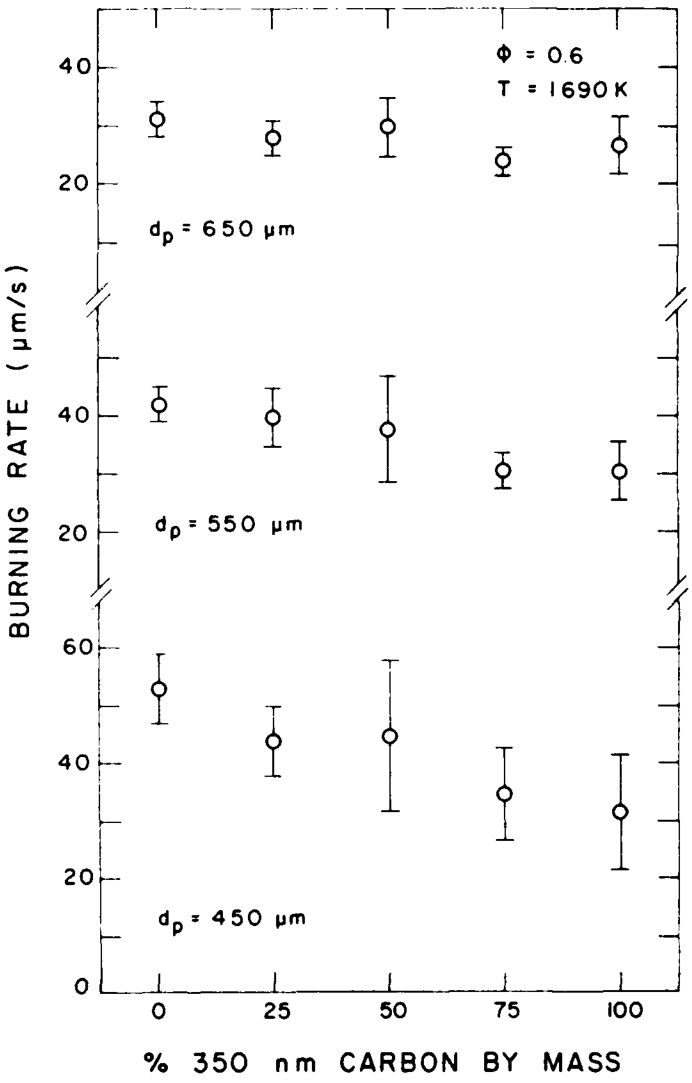

Fig. 34. Agglomerate burning rate versus carbon-black composition (d_u = 70 and 350 nm) for ϕ = 0.6, T = 1690K.

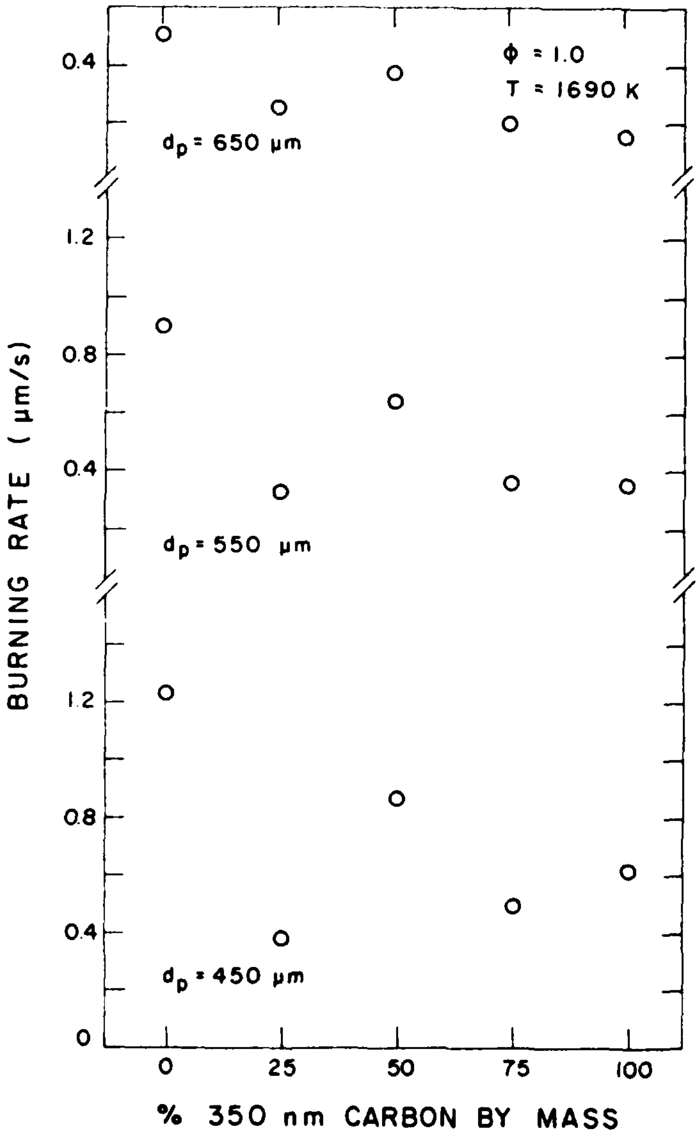

Fig. 35. Agglomerate burning rate versus carbon-black composition (d_u = 70 and 350 nm) for ϕ = 1.0, T = 1690K.

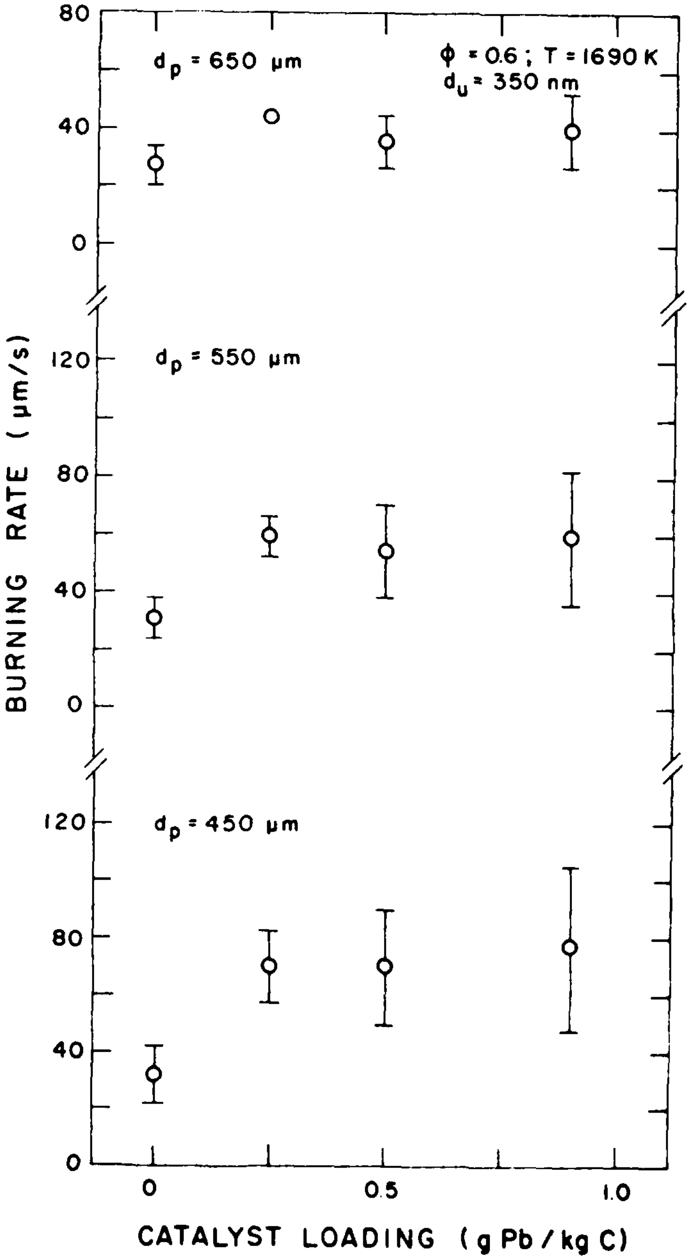

Fig. 36. Agglomerate burning rate versus lead catalyst loading (d_u = 350 nm) for φ = 0.6, T = 1690K.

relatively independent of catalyst concentration. Additional testing would be desirable in order to find optimum catalyst concentration levels.

5.4 Conclusions

Based on tests with agglomerates, having initial diameters of roughly 750 μm, supported in the post-flame region of the flat-flame burner, the following conclusions were obtained:

1. The rate of combustion of neat samples increased as the ultimate carbon particle size decreased, with maximum changes of 20-40% for d_u = 70 and 350 nm.

2. Blending samples of blacks having d_u = 70 and 350 nm yielded a monotonic variation of burning rate between the limits found for neat samples of these materials.

3. Addition of lead catalyst to a carbon black having d_u = 350 nm resulted in increased burning rates--by a factor of two in some instances. The effect of catalyst addition was greatest in the range 0-0.25 g Pb/kg C, with burning rates being relatively independent of catalyst concentration at levels higher than the upper end of this range.

4. Effects of blending and catalyst were most significant at conditions where agglomerate burning was predominantly kinetic-controlled.

5. Quantifying the present measurements concerning effects of blends and catalyst requires correlation of the data using the agglomerate combustion model developed earlier [9-14], followed by calculations using the one-dimensional combustor model described in this study.

6. Difficulties were encountered with the formation of a shell-like structure, perhaps due to contaminant or ash, for carbon-black slurries having d_u = 180 nm. Behavior of this nature had not been observed during earlier work and fuel development efforts with this material have been minimal; therefore, the practical consequence of this may not be very important. Since carbon blacks are thought to be relatively pure, however, this finding suggests that efforts to monitor impurity levels may be worthwhile.

7. Observation of surface structure at high ambient temperatures showed formation of spherical particles on the surface of agglomerates. This material is probably ash or contaminant. Achieving good atomization, and thus small agglomerates, will limit the maximum possible size of solid inert particles resulting from this process--which can be an important factor in maintaining turbomachinery components downstream of the combustor.

8. Results obtained during this investigation suggest that greatest performance improvements from fuel development efforts can be achieved by concentrating on slurry properties which can improve atomization. Drop size controls agglomerate size and small agglomerates burn more rapidly and have less potential for yielding large solid ash particles which can cause turbine wear. In particular, the one-dimensional combustor analysis suggests that agglomerate combustion occurs primarily under diffusion-controlled conditions for typical combustors and rates of burning in in this region are not strongly influenced by the fundamental reactivity of the carbon-black agglomerate.

References

1. G. W. Burdette, H. R. Lander and J. R. McCoy, "High Energy Density Fuels for Cruise Missiles," AIAA Paper No. 78-267 (1978).

2. R. H. Salveson, "Carbon Slurry Fuels for Volume Limited Missiles," Technical Report AFAPL-TR-79-2122, November 1979.

3. T. W. Bruce, H. C. Mongia, R. S. Stearns, L. W. Hall and G. M. Faeth, "Formulation, Properties and Combustion of Carbon-Slurry Fuels," Proceedings of Sixteenth JANNAF Combustion Meeting, CPIA Publication No. 308, pp. 679-717, December 1979.

4. T. W. Bruce and H. Mongia, "Compound Cycle Turbofan Engine Task IX: Carbon-Slurry Fuel Combustion Evaluation Program," Technical Report AFWAL-TR-80-2035, March 1980.

5. M. Lavid and L. A. Ruth, "The Combustion of Carbon Slurry Fuel--Experimental Results," Paper No. 6, Fall Technical Meeting--Eastern Section of The Combustion Institute, Princeton, NJ, October 1980.

6. R. S. Stearns and L. W. Hall, Jr., "Carbon Slurry Fuel Formulation and Combustion," Technical Report AFWAL-TR-82-2105, October 1982.

7. J. P. Kennedy and W. T. Peschke, "Spray Characterization and Combustion Tests of Carbon Slurry Fuels," Technical Report AFWAL-TR-81-2144, January 1982.

8. T. W. Bruce, I. Ball and H. Mongia, "Carbon Slurry Fuel Evaluation, Final Report," Technical Report, AirResearch Manufacturing Co. of Arizona, May 1982.

9. G. A. Szekely, Jr. and G. M. Faeth, "Combustion Properties of Carbon Slurry Drops," AIAA J., Vol. 20, pp. 422-429, 1982

10. G. A. Szekely, Jr., "Experimental Evaluation of a Carbon Slurry Droplet Combustion Model," Ph.D. Thesis, The Pennsylvania State University, University Park, PA, 1982.

11. G. A. Szekely and G. M. Faeth, "An Investigation of Slurry Fuel Combustion," Technical Report AFWAL-TR-80-2125, January 1981.

12. G. A. Szekely, Jr. and G. M. Faeth, "Reaction of Carbon Black Slurry agglomerates in Combustion Gases," Nineteenth Symposium (International) on Combustion, The Combustion Institute, Pittsburgh, pp. 1077-1085, 1982.

13. G. A. Szekely, Jr. and G. M. Faeth, "Combustion of Agglomerates Formed by Carbon Slurry Fuels," Technical Report AFWAL-TR-82-2085, September 1982.

14. G. A. Szekely, Jr. and G. M. Faeth, "Effects of Carbon-Black Properties on Combustion of Carbon-Black Slurry Agglomerates," submitted to Combustion and Flame.

15. G. M. Faeth, "Current Status of Droplet and Liquid Combustion," Prog. Energy Combust. Sci. Vol. 3, 191-224, 1977.

16. G. M. Faeth, "Evaporation and Combustion of Sprays," Prog. Energy Combust. Sci., Vol. 9, pp. 1-76, 1983.

17. K. G. Neoh, J. B. Howard and A. F. Sarofim, "Soot Oxidation in Flames," Particulate Carbon Formation During Combustion, D. C. Seigla and G. W. Smith, ed., Plenum Press, New York, pp. 261-282, 1981.

18. P. A. Libby and T. R. Blake, "Theoretical Study of Burning Carbon Particles," Combustion and Flame Vol. 36, 139-169, 1979.

19. P. A. Libby and T. R. Blake, "Burning Carbon Particles in the Presence of Water Vapor," Combustion and Flame, Vol. 41, pp. 123-147, 1981.

20. C. Olikara and G. L. Borman, "A Computer Program for Calculating Properties of Equilibrium Combustion Products with Some Applications to I. C. Engines," SAE Paper 750468, presented at the 1975 SAE Congress and Exposition, Feb. 24-28, 1975.

21. J. H. Lienesch and R. B. Krieger, "A Procedure to Compute Composition and Gas Properties of Equilibrium Combustion Products," Research Publication GMR-3606, General Motors Research Laboratories, Warren, MI, Mar. 10, 1981.

22. F. M. White, Viscous Fluid Flow, McGraw-Hill, New York, p. 209, 1974.

APPENDIX A

Tabulation of Data

A.1 Results for $\phi = 0.6$, $T = 1690$ K

A.1.1 Typical Particle Diameter Histories

Agglomerate Diameter Versus Time
$\phi = 0.6$, $T = 1690\text{K}$, $d_u = 70$ nm

Run 1		Run 2		Run 3		Run 4	
Time (s)	d_p (μm)	Time (s)	d_p (μm)	Time (s)	d_p (μm)	Time (s)	d_p (μm)
0.0	728	0.0	735	0.0	734	0.0	735
1.5	702	0.5	729	0.5	721	0.5	715
2.0	700	1.5	692	1.5	686	1.0	693
2.5	700	2.0	675	2.0	686	1.5	680
3.0	682	2.5	676	2.5	667	2.0	679
3.5	678	3.0	651	3.0	647	2.5	669
4.0	646	3.5	630	3.5	624	3.5	648
4.5	615	4.0	612	4.0	623	4.5	604
5.0	605	4.5	602	5.0	589	5.0	597
5.5	583	5.0	585	5.5	560	5.5	569
6.0	570	5.5	553	6.0	518	6.0	564
6.5	553	6.0	537	6.5	519	6.5	531
7.0	531	6.5	536	7.0	482	7.0	514
7.5	512	7.0	514	7.5	455	7.5	501
8.0	493	7.5	507	8.0	434	8.0	460
8.5	468	8.0	487	--	--	8.5	458
9.0	425	8.5	477	--	--	9.0	406
--	--	9.0	470	--	--	--	--
--	--	9.5	444	--	--	--	--
--	--	10.0	430	--	--	--	--
--	--	10.5	415	--	--	--	--

A.1 Results for ϕ = 0.6, T = 1690 K (Continued)

A.1.1 Typical Particle Diameter Histories

Agglomerate Diameter Versus Time
ϕ = 0.6, T = 1690 K, d_u = 70 nm and 350 nm
for a Blend of 25% 350 nm Carbon by Mass/75% 70 nm Carbon by Mass

Run 1		Run 2		Run 3		Run 4	
Time (s)	d_p (µm)	Time (s)	d_p (µm)	Time (s)	d_p (µm)	Time (s)	d_p (µm)
0.0	746	1.2	746	0.0	725	0.0	736
0.6	745	1.8	745	0.6	713	0.5	735
1.8	724	2.4	707	1.2	689	2.5	723
2.4	694	3.0	682	2.4	674	3.0	711
3.0	691	3.6	659	3.0	659	3.5	698
4.2	660	4.8	646	3.6	660	4.0	673
4.8	610	5.4	611	4.2	621	4.5	663
5.4	612	6.0	604	4.8	619	5.0	648
6.0	692	6.6	596	5.4	586	5.5	637
6.6	586	7.2	553	6.0	572	6.0	612
7.2	551	7.8	535	6.6	566	6.5	595
7.8	539	8.4	507	7.2	553	7.0	588
8.4	521	9.0	445	7.8	518	7.5	562
9.0	492	9.6	413	8.4	511	8.0	555
9.6	458	--	--	9.0	458	8.5	535
10.2	426	--	--	9.6	457	9.0	507
10.8	416	--	--	10.2	435	9.5	486
--	--	--	--	--	--	10.0	466
--	--	--	--	--	--	10.5	448
--	--	--	--	--	--	11.0	414

A.1 Results for ϕ = 0.6, T = 1690 K (Continued)

A.1.1 Typical Particle Diameter Histories

Agglomerate Diameter Versus Time
ϕ = 0.6, T = 1690 K, d_u = 70 nm and 350 nm
for a Blend of 50% 350 nm Carbon by Mass/50% 70 nm Carbon by Mass

Run 1		Run 2		Run 3		Run 4	
Time (s)	d_p (μm)	Time (s)	d_p (μm)	Time (s)	d_p (μm)	Time (s)	d_p (μm)
0.0	760	0.0	787	0.0	754	0.0	789
0.6	755	1.2	787	1.2	754	0.5	789
1.2	730	1.8	775	3.0	753	1.5	760
2.4	707	2.4	768	3.6	737	2.5	741
3.6	693	3.0	759	4.2	714	3.0	731
4.2	687	3.6	716	5.4	703	3.5	717
4.8	651	4.2	710	6.0	677	4.0	709
6.0	648	4.8	692	6.6	655	4.5	685
6.6	625	5.4	648	7.2	635	5.0	664
7.2	609	6.0	627	7.8	626	5.5	641
7.8	586	6.6	623	8.4	599	6.0	628
8.4	559	7.2	593	9.0	590	6.5	610
9.0	533	7.8	565	9.6	571	7.0	594
9.6	527	8.4	520	10.2	530	7.5	582
10.2	499	9.0	494	10.8	513	8.0	552
10.8	473	9.6	471	11.4	471	8.5	537
11.4	453	10.2	455	12.0	414	9.0	519
12.0	428	10.8	427	--	--	9.5	501
--	--	11.4	417	--	--	10.0	475
--	--	--	--	--	--	10.5	455
--	--	--	--	--	--	11.0	435
--	--	--	--	--	--	11.5	400

A.1 Results for ϕ = 0.6, T = 1690 K (Continued)

A.1.1 Typical Particle Diameter Histories

Agglomerate Diameter Versus Time
ϕ = 0.6, T = 1690 K, d_u = 70 nm and 350 nm
for a Blend of 75% 350 nm Carbon by Mass/25% 70 nm Carbon by Mass

Run 1		Run 2		Run 3		Run 4	
Time (s)	d_p (μm)	Time (s)	d_p (μm)	Time (s)	d_p (μm)	Time (s)	d_p (μm)
0	--	0.0	725	0.0	748	0.0	755
0.6	700	0.6	--	1.5	734	0.6	750
1.2	676	1.2	704	3.0	717	1.8	743
1.8	673	1.8	690	3.5	705	2.4	717
2.4	662	2.4	691	4.0	702	3.0	712
3.0	--	3.0	662	4.5	663	3.6	685
3.6	651	3.6	652	5.0	653	4.2	654
4.2	626	4.2	646	5.5	642	5.4	623
4.8	599	4.8	620	6.0	630	6.6	620
5.4	592	5.4	600	7.0	609	7.2	585
6.0	570	6.0	587	7.5	603	8.4	581
6.6	555	6.6	580	8.0	599	9.6	519
7.2	529	7.2	569	8.5	568	10.2	491
7.8	504	7.8	561	9.0	554	10.8	492
8.4	476	8.4	526	9.5	545	11.4	456
9.0	473	9.0	495	10.0	526	12.0	429
9.6	422	9.6	483	10.5	510	12.6	420
--	--	10.2	482	11.0	506	--	--
--	--	10.8	442	11.5	493	--	--
--	--	11.4	433	12.0	479	--	--
--	--	--	--	12.5	461	--	--
--	--	--	--	13.0	455	--	--
--	--	--	--	13.5	430	--	--
--	--	--	--	14.0	417	--	--

A.1 Results for ϕ = 0.6, T = 1690 K (Continued)

A.1.1 Typical Particle Diameter Histories

Agglomerate Diameter Versus Time
ϕ = 0.6, T = 1690 K, d_u = 350 nm

Run 1		Run 2		Run 3		Run 4	
Time (s)	d_p (μm)	Time (s)	d_p (μm)	Time (s)	d_p (μm)	Time (s)	d_p (μm)
0	743	0	741	0	757	0	729
1.4	738	1.4	692	1.8	728	.7	727
2.1	706	2.8	681	2.4	723	1.4	714
2.8	705	3.5	659	3.0	692	2.1	699
3.5	690	4.2	635	4.2	667	2.8	682
4.2	673	4.9	623	4.8	642	3.5	665
4.9	665	5.6	595	5.4	637	4.2	630
5.6	625	7.0	578	6.0	609	4.9	622
6.3	585	7.7	568	6.6	599	5.6	591
7.0	585	8.4	536	7.2	586	6.3	581
7.7	549	9.8	491	7.8	562	7.0	581
8.4	528	11.2	448	8.4	537	7.7	558
9.1	495	11.9	444	9.0	531	8.4	527
9.8	467	12.6	421	9.6	513	9.1	503
10.5	447	--	--	10.2	503	9.8	472
11.2	432	--	--	10.8	482	10.5	418
11.9	421	--	--	11.4	458	11.2	405
--	--	--	--	12.6	424	--	--

A.1 Results for $\phi = 0.6$, T = 1690 K (Continued)

A.1.2 Burning Rates

Agglomerate Burning Rate
$\phi = 0.6$, T = 1690 K

d_p (μm)	$-BR$ $\left(\frac{\mu m}{s}\right)$	σ_{BR} $\left(\frac{\mu m}{s}\right)$
70 nm Slurry		
700	26.2	3.9
650	30.7	3.0
600	35.2	3.6
550	41.9	2.7
500	47.6	2.7
450	53.0	5.6
25% 350 nm C by Mass/75% 70 nm C by Mass		
700	21.6	1.1
650	27.8	2.6
600	33.8	7.3
550	39.4	5.2
500	40.8	4.5
450	44.3	5.7
50% 350 nm C by Mass/50% 70 nm C by Mass		
700	25.5	7.6
650	30.0	4.8
600	34.1	4.7
550	38.0	8.7
500	41.5	9.4
450	45.0	12.6
75% 350 nm C by Mass/25% 70 nm C by Mass		
700	18.5	4.6
650	23.8	1.6
600	27.6	1.0
550	30.5	3.2
500	32.9	5.5
450	34.7	8.2
350 nm Slurry		
700	25.2	2.6
650	26.8	4.6
600	30.6	5.4
550	31.1	4.9
500	32.2	5.9
450	31.8	9.9

A.2 Results for $\phi = 0.6$, T = 1940 K

A.2.1 Typical Particle Diameter Histories

Agglomerate Diameter Versus Time
$\phi = 0.6$, T = 1940 K, d_u = 70 nm

Run 1		Run 2		Run 3		Run 4	
Time (s)	d_p (μm)	Time (s)	d_p (μm)	Time (s)	d_p (μm)	Time (s)	d_p (μm)
0	741	0	744	0	741	0	774
0.9	746	0.3	744	0.3	743	0.6	774
1.2	722	1.2	742	0.6	734	1.2	773
1.5	706	1.5	707	0.9	721	1.5	747
1.8	701	1.8	703	1.2	708	1.8	725
2.1	675	2.1	677	1.5	687	2.1	707
2.4	660	2.4	642	1.8	660	2.4	674
2.7	634	2.7	625	2.1	643	2.7	658
3.0	629	3.0	609	2.4	633	3.0	647
3.3	598	3.3	585	2.7	621	3.3	636
3.6	591	3.6	585	3.0	593	3.6	598
3.9	574	3.9	565	3.3	572	3.9	601
4.2	530	4.2	537	3.6	543	4.2	562
4.5	509	4.5	501	3.9	534	4.5	530
4.8	483	4.8	498	4.2	499	4.8	510
5.1	449	5.1	470	4.5	500	5.1	483
5.4	441	5.4	438	4.8	474	5.4	466
5.7	412	5.7	421	5.1	450	5.7	407
--	--	--	--	5.4	420	--	--
--	--	--	--	5.7	403	--	--

A.2 Results for ϕ = 0.6, T = 1940 K (Continued)

A.2.1 Typical Particle Diameter Histories

Agglomerate Diameter Versus Time
$\phi = 0.6$, T = 1940 K, d_u = 70 nm and 350 nm
for a Blend of 25% 350 nm Carbon by Mass/75% 70 nm Carbon by Mass

Run 1		Run 2		Run 3		Run 4	
Time (s)	d_p (μm)	Time (s)	d_p (μm)	Time (s)	d_p (μm)	Time (s)	d_p (μm)
0	752	0	737	0	784	0	740
0.8	747	0.4	722	0.8	784	0.4	737
1.2	732	1.6	703	1.2	778	1.2	721
1.6	736	2.0	670	1.6	753	1.6	699
2.0	723	2.4	670	2.0	722	2.0	688
2.4	700	2.8	638	2.4	687	2.4	668
2.8	669	3.2	612	2.8	675	2.8	637
3.2	657	3.6	600	3.2	650	3.2	637
3.6	631	4.0	583	3.6	626	3.6	602
4.0	602	4.4	558	4.0	578	4.0	580
4.4	598	4.8	536	4.4	559	4.4	574
4.8	574	5.2	517	4.8	526	4.8	546
5.2	556	5.6	490	5.2	501	5.2	529
5.6	511	6.0	467	5.6	467	5.6	513
6.0	512	6.4	436	6.0	412	6.0	488
6.4	482	--	--	6.4	400	6.4	455
6.8	453	--	--	--	--	6.8	426
7.2	443	--	--	--	--	--	
7.6	414	--	--	--	--	--	

A.2 Results for ϕ = 0.6, T = 1940 K (Continued)

A.2.1 Typical Particle Diameter Histories

Agglomerate Diameter Versus Time
ϕ = 0.6, T = 1940 K, d_u = 70 nm and 350 nm
for a Blend of 50% 350 nm Carbon by Mass/50% 70 nm Carbon by Mass

Run 1		Run 2		Run 3		Run 4	
Time (s)	d_p (μm)	Time (s)	d_p (μm)	Time (s)	d_p (μm)	Time (s)	d_p (μm)
0	741	0	763	0	741	0	784
0.3	734	0.8	769	0.4	741	0.8	776
0.6	723	1.2	740	0.8	738	1.2	764
0.9	708	1.6	731	1.2	734	1.6	755
1.5	689	2.0	726	1.6	727	2.0	744
1.8	676	2.4	716	2.0	709	2.4	717
2.1	660	2.8	680	2.4	680	2.8	707
2.4	641	3.2	661	2.8	659	3.2	685
2.7	623	3.6	648	3.2	637	3.6	658
3.0	614	4.0	634	3.6	629	4.0	648
3.3	586	4.4	608	4.0	586	4.4	630
3.6	572	4.8	589	4.4	560	4.8	627
3.9	548	5.2	581	4.8	544	5.2	599
4.2	547	5.6	558	5.2	518	5.6	572
4.5	531	6.0	544	5.6	490	6.0	554
4.8	5.0	6.4	514	6.0	458	6.4	535
5.1	466	6.8	497	6.4	434	6.8	514
5.6	458	7.2	471	--	--	7.2	477
5.7	437	7.6	457	--	--	7.6	475
6.0	421	8.0	410	--	--	8.0	450
--	--	8.4	404	--	--	8.4	403

A.2 Results for ϕ = 0.6, T = 1940 K (Continued)

A.2.1 Typical Particle Diameter Histories

Agglomerate Diameter Versus Time
$\phi = 0.6$, T = 1940 K, d_u = 70 nm and 350 nm
for a Blend of 75% 350 nm Carbon by Mass/25% 70 nm Carbon by Mass

Run 1		Run 2		Run 3		Run 4	
Time (s)	d_p (μm)	Time (s)	d_p (μm)	Time (s)	d_p (μm)	Time (s)	d_p (μm)
0	768	0	740	0	750	0	747
0.8	768	1.0	732	0.4	741	0.4	741
1.2	763	1.5	722	0.8	739	0.8	711
1.6	756	2.0	681	1.6	728	1.2	712
2.0	725	2.5	677	2.0	713	2.0	702
2.4	708	3.0	660	2.4	697	2.4	669
2.8	694	3.5	611	2.8	683	2.8	642
3.2	672	4.0	590	3.2	657	3.2	642
3.6	667	4.5	554	3.6	654	3.6	627
4.0	632	5.0	519	4.0	621	4.0	614
4.4	601	5.5	476	4.4	591	4.4	587
4.8	588	6.0	467	4.8	564	4.8	569
5.2	567	6.5	429	5.2	547	5.2	566
5.6	546	--	--	5.6	529	5.6	536
6.0	531	--	--	6.0	514	6.0	532
6.4	507	--	--	6.4	476	6.4	493
6.8	491	--	--	6.8	454	6.8	474
7.2	467	--	--	7.2	420	7.2	461
7.6	429	--	--	7.6	412	7.6	436
8.0	429	--	--	--	--	8.0	406

A.2 Results for ϕ = 0.6, T = 1940 K (Continued)

A.2.1 Typical Particle Diameter Histories

Agglomerate Diameter Versus Time
$\phi = 0.6$, T = 1940 K, d_u = 350 nm

Run 1		Run 2		Run 3		Run 4	
Time (s)	d_p (μm)	Time (s)	d_p (μm)	Time (s)	d_p (μm)	Time (s)	d_u (μm)
0	761	0	748	0	742	0	740
0.3	761	0.4	736	0.8	742	0.4	737
1.8	747	0.8	737	1.2	738	0.8	724
2.4	735	1.2	732	1.6	737	1.6	725
2.7	723	1.6	723	2.0	712	2.0	714
3.0	706	2.0	687	2.4	695	2.4	701
3.3	692	2.8	675	2.8	672	2.8	681
3.6	684	3.2	657	3.2	652	3.2	672
3.9	674	3.6	640	3.6	621	3.6	656
4.2	641	4.0	625	4.0	613	4.0	590
4.5	644	4.4	600	4.4	585	4.4	571
4.8	603	4.8	588	4.8	570	4.8	536
5.1	597	5.2	562	5.2	536	5.2	505
5.4	593	5.6	556	5.6	501	5.6	470
5.7	567	6.0	527	6.0	497	6.0	437
6.0	549	6.4	516	6.4	470	6.4	402
6.3	513	6.8	489	6.8	438	--	--
6.6	499	7.2	468	7.2	426	--	--
6.9	484	7.6	441	--	--	--	--
7.2	455	8.0	426	--	--	--	--
7.5	446	8.4	404	--	--	--	--
7.8	430	--	--	--	--	--	--
8.1	404	--	--	--	--	--	--

A.2 Results for ϕ = 0.6, T = 1940 K (Continued)

A.2.2 Burning Rates

Agglomerate Burning Rate
ϕ = 0.6, T = 1940 K

d_p (μm)	-BR $(\frac{\mu m}{s})$	σ_{BR} $(\frac{\mu m}{s})$
70 nm Slurry		
700	51.7	4.7
650	64.9	3.9
600	72.8	4.8
550	77.3	6.5
500	79.1	8.9
450	78.4	12.4
25% 350 nm C by Mass/75% 70 nm C by mass		
700	36.8	4.3
650	46.7	4.8
600	52.7	4.1
550	56.3	2.1
500	58.0	1.8
450	57.8	6.6
50% 350 nm C by Mass/50% 70 nm C by Mass		
700	40.9	2.3
650	51.1	5.4
600	55.6	7.2
550	59.1	7.0
500	60.8	5.8
450	60.8	4.9
75% 350 nm C by Mass/25% 70 nm C by Mass		
700	39.8	5.3
650	49.4	8.7
600	54.7	9.4
550	57.2	8.2
500	57.3	6.0
450	54.5	3.2
350 nm Slurry		
700	39.7	6.5
650	50.2	8.3
600	56.0	8.6
550	58.6	8.1
500	58.8	7.2
450	56.0	8.0

A.3 Results for $\phi = 1.0$, T = 1690 K

A.3.1 Typical Particle Diameter Histories

Agglomerate Diameter Versus Time
$\phi = 1.0$, T = 1690 K, $d_u = 70$ nm

Time (s)	d_p (μm)
0.0	749
90	749
135	732
270	723
360	709
405	691
450	691
495	675
540	646
585	641
630	572
675	564
720	521
765	464

A.3 Results for ϕ = 1.0, T = 1690 K (Continued)

A.3.1 Typical Particle Diameter Histories

Agglomerate Diameter Versus Time
ϕ = 1.0, T = 1690 K, d_u = 70 nm and 350 nm
for a Blend of 25% 350 nm Carbon by Mass/
75% 70 nm Carbon by Mass

Time (s)	d_p (μm)
0.0	744
45	744
135	733
180	727
315	727
360	713
405	713
450	700
495	694
540	687
585	684
630	678
675	655
720	643
765	635
810	619
855	597
900	606
945	566
990	565
1035	556
1080	538
1125	522
1170	522
1215	485
1260	470
1305	460
1350	437

A.3 Results for ϕ = 1.0, T = 1690 K (Continued)

A.3.1 Typical Particle Diameter Histories

Agglomerate Diameter Versus Time
ϕ = 1.0, T = 1690 K, d_u = 70 nm and 350 nm
for a Blend of 50% 350 nm Carbon by Mass/
50% 70 nm Carbon by Mass

Time (s)	d_p (μm)
0.0	761
45	754
135	751
180	755
270	737
360	730
495	708
540	706
630	695
675	694
765	670
810	632
855	625
900	588
945	562
990	558
1035	507
1080	485

AD-A136 390 COMBUSTION OF AGGLOMERATES FORMED BY CARBON SLURRY FUELS(U) PENNSYLVANIA STATE UNIV UNIVERSITY PARK DEPT OF MECHANICAL ENGINEERING S R TURNS ET AL. NOV 83

UNCLASSIFIED AFWAL-TR-83-2076 F33615-82-K-2256 F/G 21/2 NL

2/2

END
DATE
FILMED
1-84
DTIC

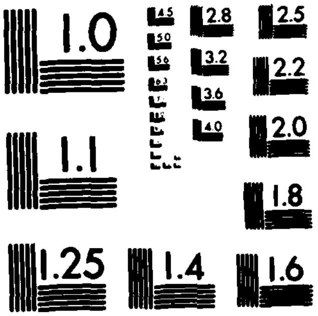

MICROCOPY RESOLUTION TEST CHART
NATIONAL BUREAU OF STANDARDS 1963 A

A.3 Results for ϕ = 1.0, T = 1690 K (Continued)

A.3.1 Typical Particle Diameter Histories

Agglomerate Diameter Versus Time
$\phi = 1.0$, T = 1690 K, $d_u = 70$ nm and 350 nm
for a Blend of 75% 350 nm Carbon by Mass/
25% 70 nm Carbon by Mass

Time (s)	d_p (μm)
0.0	753
45	753
180	747
225	744
270	741
315	733
360	728
450	728
495	729
540	711
585	707
630	710
675	705
765	706
855	700
900	686
945	673
990	663
1080	639
1125	629
1170	628
1215	625
1260	600
1305	586
1395	559
1440	551
1485	523
1530	504

A.3 Results for ϕ = 1.0, T = 1690 K (Continued)

A.3.1 Typical Particle Diameter Histories

Agglomerate Diameter Versus Time
ϕ = 1.0, T = 1690 K, d_u = 70 350 nm

Time (s)	d_p (μm)
0.0	743
90	711
180	685
225	674
270	660
360	647
405	644
495	631
585	631
630	608
675	594
720	590
765	587
810	562
855	549
900	546
945	516
990	490
1035	484
1080	446
1125	415

A.3 Results for ϕ = 1.0, T = 1690 (Continued)

A.3.2 Burning Rates

Agglomerate Burning Rate
ϕ = 1.0, T = 1690 K

d_p (μm)	$-BR$ ($\frac{\mu m}{s}$)
70 nm Slurry	
700	0.25
650	0.51
600	0.71
550	0.90
500	1.07
450	1.23
25% 350 nm C by Mass/75% 70 nm C by Mass	
700	0.18
650	0.25
600	0.30
550	0.33
500	0.36
450	0.38
50% 350 nm C by Mass/50% 70 nm C by Mass	
700	0.20
650	0.37
600	0.51
550	0.64
500	0.76
450	0.86
75% 350 nm C by Mass/25% 70 nm C by Mass	
700	0.11
650	0.20
600	0.28
550	0.36
500	0.43
450	0.49
350 nm Slurry	
700	0.28
650	0.15
600	0.21
550	0.35
500	0.49
450	0.62

A.4 Results for Catalyst Loading

A.4.1 Typical Particle Histories

Agglomerate Diameter Versus Time
$\phi = 0.6$, $T = 1690$ K, $d_u = 350$ nm

0.25 $\frac{g\ Pb}{Kg\ C}$				0.50 $\frac{g\ Pb}{Kg\ C}$			
Run 1		Run 2		Run 1		Run 2	
Time (s)	d_p (μm)	Time (s)	d_p (μm)	Time (s)	d_p (μm)	Time (s)	d_p (μm)
0.0	736	0.0	758	0.0	730	0.0	756
0.5	732	1.0	758	0.5	727	0.5	737
1.0	735	2.0	753	1.0	713	2.5	728
1.5	720	2.5	738	1.5	704	3.0	728
2.0	727	3.0	699	2.0	696	3.5	697
2.5	717	3.5	690	2.5	663	4.0	684
3.0	694	4.0	670	3.0	658	4.5	683
3.5	684	5.0	632	3.5	655	5.0	655
4.0	665	5.5	622	4.0	632	5.5	630
4.5	658	6.0	580	4.5	598	6.0	627
5.0	646	7.0	543	5.0	585	6.5	604
5.5	606	7.5	497	6.0	560	7.0	575
6.0	556	8.0	488	6.5	527	7.5	503
6.5	535	8.5	440	7.0	508	8.0	475
7.0	513	--	--	7.5	501	8.5	452
7.5	471	--	--	8.0	475	9.0	414
8.0	440	--	--	8.5	441	--	--
8.5	390	--	--	9.0	392	--	--

A.4 Results for catalyst Loading (Continued)

A.4.1 Typical Particle Diameter Histories

Agglomerate Diameter Versus Time
$\phi = 0.6$, T = 1690 K, $d_u = 350$ nm

		$.90\ \frac{g\ Pb}{Kg\ C}$			
Run 1		Run 2		Run 3	
Time (s)	d_p (µm)	Time (s)	d_p (µm)	Time (s)	d_p (µm)
0.0	739	0.0	758	0.0	758
0.5	739	0.5	746	1.5	746
1.0	725	2.5	744	2.0	744
1.5	712	3.0	717	2.5	715
2.0	707	3.5	705	3.0	696
2.5	662	4.0	689	3.5	667
3.0	654	4.5	675	4.0	640
3.5	648	5.0	666	4.5	630
4.0	624	5.5	651	5.0	590
5.0	601	6.0	636	5.5	548
5.5	589	6.5	599	6.0	502
6.0	575	7.0	594	6.5	479
6.5	549	7.5	581	7.0	400
7.0	551	8.0	545	--	--
7.5	524	8.5	507	--	--
8.5	478	9.0	481	--	--
9.0	464	9.5	385	--	--
9.5	426	--	--	--	--
10.0	413	--	--	--	--

A.4 Results for Catalyst Loading (Continued)

A.4.2 Burning Rates

Agglomerate Burning Rate
$\phi = 0.6$, $T = 1690$ K, $d_u = 350$ nm

d_p (μm)	Burning Rates ($\frac{\mu m}{s}$) Catalyst Loading (g Pb/Kg C) 0	0.25	0.50	0.90
650	27 ± 5	43 ± 1	33 ± 9	39 ± 12
550	31 ± 5	59 ± 6	54 ± 16	59 ± 23
450	32 ± 10	70 ± 13	70 ± 21	77 ± 28

☆ U.S.Government Printing Office: 1983 — 759-062/603